Monthly Notices of the ROYAL ASTRONOMICAL SOCIETY

MNRAS **472,** 4382–4403 (2017) doi:10.1093/mnras/stx2264
Advance Access publication 2017 September 4

The first 62 AGNs observed with SDSS-IV MaNGA – I. Their characterization and definition of a control sample

Sandro B. Rembold,[1,2]★ Jáderson S. Shimoia,[2,3]★ Thaisa Storchi-Bergmann,[2,3]★ Rogério Riffel,[2,3] Rogemar A. Riffel,[1,2] Nícolas D. Mallmann,[2,3] Janaína C. do Nascimento,[2,3] Thales N. Moreira,[1,2] Gabriele S. Ilha,[1,2] Alice D. Machado,[1,2] Rafael Cirolini,[1,2] Luiz N. da Costa,[2,4] Marcio A. G. Maia,[2,4] Basílio X. Santiago,[2,3] Donald P. Schneider,[5,6] Dominika Wylezalek,[7] Dmitry Bizyaev,[8,9] Kaike Pan[8] and Francisco Müller-Sánchez[10]

[1]*Departamento de Física, CCNE, Universidade Federal de Santa Maria, 97105-900, Santa Maria, RS, Brazil*
[2]*Laboratório Interinstitucional de e-Astronomia - LIneA, Rua Gal. José Cristino 77, Rio de Janeiro, RJ - 20921-400, Brazil*
[3]*Departamento de Física, IF, Universidade Federal do Rio Grande do Sul, CP 15051, 91501-970, Porto Alegre, RS, Brazil*
[4]*Observatório Nacional - MCT, Rua General José Cristino 77, Rio de Janeiro, RJ - 20921-400, Brazil*
[5]*Institute for Gravitation and the Cosmos, The Pennsylvania State University, University Park, PA 16802, USA*
[6]*Department of Astronomy and Astrophysics, The Pennsylvania State University, University Park, PA 16802, USA*
[7]*Center for Astrophysical Sciences, Department of Physics and Astronomy, Johns Hopkins University, 3400 North Charles Street, Baltimore, MD 21218, USA*
[8]*Apache Point Observatory, PO Box 59, Sunspot, NM 88349, USA*
[9]*Sternberg Astronomical Institute, Moscow State University, 119992 Moscow, Russia*
[10]*Center for Astrophysics and Space Astronomy, Department of Astrophysical and Planetary Sciences, University of Colorado, 389 UCB, Boulder, CO 80309-0389, USA*

Accepted 2017 August 30. Received 2017 August 28; in original form 2016 July 6

ABSTRACT

We report the characterization of the first 62 Mapping Nearby Galaxies at the Apache Point Observatory active galactic nuclei (AGNs) hosts and the definition of a control sample of non-active galaxies. This control sample was selected in order to match the AGN hosts in terms of stellar mass, redshift, visual morphology and inclination. The stellar masses are in the range $9.4 < \log\left(M/\mathrm{M}_{\odot}\right) < 11.5$, and most objects have redshifts $\leq$0.08. The AGN sample is mostly comprised low-luminosity AGN, with only 17 'strong AGN' with $L([\mathrm{O\,III}]\lambda5007\,\text{Å}) \geq 3.8 \times 10^{40}\,\mathrm{erg\,s^{-1}}$. The inner 1–3 kpc of the control sample galaxies are dominated by the oldest ($\geq$ 4 Gyr) component, with a small contribution of intermediate age and young stars (<940 Myr). Examining the relationship between the stellar population properties and $L([\mathrm{O\,III}])$, we find that with increasing $L([\mathrm{O\,III}])$, the AGN exhibit a decreasing contribution from the oldest stellar population relative to control galaxies and an increasing contribution from the younger components (∼40 Myr). We also find a correlation of the mean age differences (AGN–control) with $L([\mathrm{O\,III}])$, in the sense that more luminous AGNs are younger than the control objects, while the low-luminosity AGNs are older. These results support a connection between the growth of the galaxy bulge via formation of new stars and the growth of the Supermassive Black Hole via accretion in the AGN phase.

Key words: galaxies: active – galaxies: stellar content.

1 INTRODUCTION

The MaNGA (Mapping Nearby Galaxies at the Apache Point Observatory) survey, a core program of the fourth-generation Sloan Digital Sky Survey (SDSS-IV), operating between 2014 and 2020, will deliver optical integral field spectroscopic observations of ∼10 000 galaxies. It has been conceived in order to produce homogeneous spectroscopic information of these galaxies out to a radial position of at least $1.5r_{\mathrm{e}}$ (effective radius). An overview of the main science objectives and survey design is presented in Bundy et al. (2015). The integral field unit design and performance are described in Drory et al. (2015). Details about the observing strategy in order to ensure spectrophotometric accuracy are given in Law et al. (2015). The spectrophotometric calibration technique is described in Yan et al. (2016).

★ E-mail: sandro.rembold@ufsm.br (SBR); silva.schimoia@ufrgs.br (JS); thaisa@ufrgs.br (TS-B)

Among the 10 000 galaxies, there are expected to be ∼300 galaxies hosting active galactic nuclei (AGNs). One of the primary goals of the MaNGA survey is to explore the relation between the AGN and their host galaxies. This investigation will be accomplished via the mapping of the ionized and neutral gas kinematics, searching in particular for outflows and investigating the corresponding feedback effects on the host galaxy (Zakamska & Greene 2014). The empirical relationship between the mass of the central Supermassive Black Hole (SMBH) in AGNs and the stellar velocity dispersion of the spheroidal component of galaxies (the $M_\bullet$–σ relationship) suggests that the growth of a galaxy (due to star formation) and its central SMBH (due to gas accretion) may be coupled (e.g. Ferrarese & Merrit 2000; Gebhardt et al. 2000), although some non-causal explanations have been also recently proposed (e.g. Peng 2007; Jahnke & Macciò 2011). The observed $M_\bullet - \sigma$ relationship has been explained as being originated by the AGN feeding and feedback processes that couple the growth of the SMBHs and their host galaxies (Ferrarese & Ford 2005; Somerville et al. 2008; Kormendy & Ho 2013). Indeed, cosmological simulations suggest that AGN plays a fundamental role in the evolution of its host galaxy (Di Matteo, Springel & Hernquist 2005; Springel, Di Matteo & Hernquist 2005; Bower et al. 2006), as while the SMBH evolves together with the galaxy, it is fed by surrounding material and periodically produces gas ejections that retard the growth of the galaxy by preventing the accretion of extragalactic gas in these active phases (e.g. Nemmen et al. 2007; Fabian et al. 2012; Terrazas et al. 2016).

AGN feeding and feedback effects are related to the stellar population of the host galaxy. Previous studies have suggested that the feeding, leading to the growth of the central SMBH, appears to be related to recent episodes of star formation in the circumnuclear region (e.g. Heckman et al. 1997; Storchi-Bergmann et al. 2001; Davies et al. 2007; Hickox et al. 2014; Diamond-Stainic & Rieke 2012; Esquej et al. 2014). These studies found an excess of young to intermediate age stars in the inner few hundred parsecs of AGN hosts when compared to non-active galaxies and support the existence of an AGN-Starburst connection (Perry & Dyson 1985; Terlevich & Melnick 1985; Norman & Scoville 1988). This connection can be understood, as both star formation and nuclear activity may be fed by gas inflows towards de centre or, alternatively the central AGN may be triggered due to mass-loss from evolving stars (e.g. Wild, Heckman & Charlot 2010). The AGN feedback, both via radiative and kinetic power, may, in turn, also affect the stellar populations of the host galaxy in the vicinity of the AGN by quenching star formation (e.g. Fabian et al. 2012; Dubois et al. 2013; Ishibashi & Fabian 2017; Pontzen et al. 2017; Xie, Yuan & Ho 2017).

This study is the first of a series of papers in which we will use the MaNGA data cubes to obtain the properties of AGN and a matched sample of inactive galaxies. We have so far used the 2778 galaxy data cubes released in the 5th MaNGA Product Launch (MPL-5), obtained between 2014 and 2016. The cubes have been processed using the version 2.0.1 of the MaNGA Data Reduction Pipeline Law et al. (2016). This set of data cubes contains 62 AGN hosts, selected using optical emission-line diagnostics as described in Section 2.1, comprising 45 low-luminosity ($L_{[\mathrm{O\,III}]} < 3.8 \times 10^{40}$ erg s^{-1}) AGNs and 17 higher luminosity ones from both the baseline MaNGA sample and the Ancillary AGN sample.[1]

Our goal with this first paper is to broadly characterize the properties of this initial AGN sample and select a control sample of inactive galaxies matched to the AGN hosts in absolute magnitude, galaxy mass, redshift, galaxy type and inclination. The definition of a control sample is essential in order to investigate the effects of AGN feeding and feedback on the host galaxy properties, and in order to do this, it is necessary to make sure that eventual differences are not related to properties such as Hubble type or galaxy mass. We have found so far 62 AGNs and 109 control sample galaxies, but the criteria introduced in this paper will be used to increase our sample to at least 300 AGNs (estimated to be observed) and corresponding control sample galaxies by the conclusion of the MaNGA survey.

Besides presenting and characterizing the AGN and control samples, we investigate the similarities and differences between the stellar populations of the two samples. This study was performed in two steps: In this paper, we compare the stellar population of the AGN hosts and control galaxies using stellar population synthesis of the nuclear spectra over the inner 3 arcsec from the SDSS-III survey (Gunn et al. 2006; Eisenstein et al. 2011; Smee et al. 2013). In a forthcoming paper (Mallmann et al., in preparation), we will use the MaNGA data cubes to compare the resolved stellar population properties up to $1.5r_e$.

This paper is organized as follows. In Section 2, we present and describe the AGN and control samples; in Section 3, we compare the properties of the two samples; in Section 4, we describe the stellar population synthesis method; in Section 5, we discuss the results and in Section 6 we present our conclusions. We have assumed a cosmology with $H_0 = 70\,\mathrm{km\,s^{-1}\,Mpc^{-1}}$, $\Omega_\mathrm{m} = 0.3$ and $\Omega_V = 0.7$.

2 SAMPLE SELECTION AND CHARACTERIZATION

2.1 Galaxies hosting an active nucleus

AGN produce a spectral energy distribution consistently harder than massive main-sequence stars. A common tool for identifying the origin of the ionizing photons in optical emission-line galaxies (active nuclei, starbursts or transition objects) is the BPT diagram (Baldwin, Phillips & Terlevich 1981), which is based on line ratios between high- and low-ionization potential species. But one weakness of the BPT diagram is its inability to discriminate between a genuine low-ionization AGN and emission-line galaxies, whose ionizing photons are produced in the atmospheres of evolved low-mass stars (the so-called post-AGB stars). In order to circumvent this limitation, Cid Fernandes et al. (2010) have introduced a new diagnostic diagram that makes use of the equivalent width of Hα (EWHα) – the so-called WHAN diagram. These authors have shown that galaxies that have $\mathrm{EW_{H\alpha}}$ smaller than 3 Å are not ionized by AGNs but instead are ionized by post-AGB stars, and have been dubbed 'LIERS'.

In order to identify hosts of 'true' AGN in the MaNGA MPL-5 sample, we have made use of the BPT and the WHAN diagrams simultaneously. We have cross-matched all galaxy data cubes observed in MPL-5 with the SDSS-III spectroscopic data from DR12 (Alam et al. 2015). We have obtained line fluxes and equivalent widths of Hβ, Hα, [O III] λ5007 and [N II] λ6584, measured in the

[1] As the baseline MaNGA sample contains limited dynamic range in AGN luminosity, reaching only $L([\mathrm{O\,III}]) \approx 10^{40}$ erg s^{-1} ($L_\mathrm{bol} \approx 10^{43}$ erg s^{-1}), it is not well suited to explore the relationship between the AGN power and both the outflows and stellar populations of the host galaxy. In order to address this issue, an auxiliary program to cover a wider range of AGN luminosities was proposed by a group led by PI Jenny Greene. This successful proposal will lead to the observation of an additional ≈150 AGN with luminosities up to $L_\mathrm{bol} \approx 10^{45}$ erg s^{-1}.

Table 1. Parameters of AGN in MaNGA-MPL5. (1) galaxy identification in the MaNGA survey; (2) MaNGA plate-IFU identification of the observation; (3)–(4): RA/Dec. (2000) in degrees; (5) spectroscopic redshift from SDSS-III; (6): integrated absolute *r*-band magnitude from SDSS-III; (7): stellar mass in units of $M_{\odot}$; errors associated with the stellar masses of galaxies in our sample are typically under 0.03 dex (Conroy, Gunn & White 2009); (8) elliptical/spiral/merging classification from Galaxy Zoo I; (9)–(10): *r*-band concentration and asymmetry derived with PYCA; and (11) [O III] luminosity in units of 10^{40} erg s^{-1}.

mangaID (1)	RA (2)	Dec. (3)	z (4)	M_r (5)	log $M^{\star}/M_{\odot}$ (6)	GZ1$_c$ (7)	C (8)	A (9)	L([O III]) (10)
1-558912	166.129 410	42.624 554	0.1261	− 20.46	11.25	–	0.37	0.12	56.82 ± 1.25
1-269632	247.560 974	26.206 474	0.1315	− 21.78	11.62	S	0.47	0.05	30.08 ± 1.69
1-258599	186.181 000	44.410 770	0.1256	− 21.24	11.68	E	0.50	0.11	20.95 ± 0.67
1-72322	121.014 198	40.802 612	0.1262	− 21.81	12.05	S	0.34	0.08	20.66 ± 0.43
1-121532	118.091 110	34.326 569	0.1400	− 20.51	11.34	E	0.33	0.05	11.68 ± 0.96
1-209980	240.470 871	45.351 940	0.0420	− 19.70	10.79	S	0.57	0.04	11.01 ± 0.17
1-44379	120.700 706	45.034 554	0.0389	− 19.89	10.97	S	0.24	0.06	8.94 ± 0.14
1-149211	168.947 800	50.401 634	0.0473	− 18.27	10.16	S	0.29	0.03	7.88 ± 0.14
1-173958	167.306 015	49.519 432	0.0724	− 20.53	11.31	S	0.33	0.06	6.79 ± 0.30
1-338922	114.775 749	44.402 767	0.1345	− 20.27	11.13	M	0.44	0.03	6.77 ± 0.90
1-279147	168.957 733	46.319 565	0.0533	− 19.51	10.66	S	0.45	0.03	6.77 ± 0.20
1-460812	127.170 799	17.581 400	0.0665	− 19.81	11.44	–	0.38	0.05	6.46 ± 0.31
1-92866	243.581 818	50.465 611	0.0603	− 20.56	11.69	E	0.49	0.05	6.12 ± 0.30
1-94784	249.318 420	44.418 228	0.0314	− 20.06	10.85	S	0.42	0.03	5.96 ± 0.12
1-44303	119.182 152	44.856 709	0.0499	− 19.72	10.62	S	0.29	0.10	5.56 ± 0.12
1-339094	117.472 420	45.248 482	0.0313	− 19.02	10.52	E	0.36	0.03	5.29 ± 0.09
1-137883	137.874 756	45.468 319	0.0268	− 18.06	10.77	E/S	0.41	0.01	3.87 ± 0.12
1-48116	132.653 992	57.359 669	0.0261	− 19.18	10.60	S	0.31	0.06	3.79 ± 0.08
1-256446	166.509 872	43.173 473	0.0584	− 19.40	11.14	E	0.49	0.05	3.74 ± 0.15
1-95585	255.029 877	37.839 500	0.0633	− 20.88	11.24	S	0.27	0.08	3.58 ± 0.16
1-135641	249.557 312	40.146 820	0.0304	− 19.03	11.19	S	0.28	0.08	3.52 ± 0.09
1-259142	193.703 995	44.155 567	0.0543	− 20.75	11.29	S	0.39	0.06	3.47 ± 0.20
1-109056	39.446 587	0.405 085	0.0473	− 19.27	10.57	–	0.32	0.05	3.24 ± 0.08
1-24148	258.827 423	57.658 772	0.0282	− 18.51	10.56	S	0.31	0.04	3.17 ± 0.05
1-166919	146.709 106	43.423 843	0.0722	− 20.85	11.28	S	0.37	0.06	2.64 ± 0.25
1-248389	240.658 051	41.293 427	0.0348	− 19.36	10.57	S	0.49	0.12	2.55 ± 0.09
1-321739	226.431 656	44.404 903	0.0283	− 18.91	11.12	S	0.40	0.14	2.24 ± 0.10
1-234618	202.128 433	47.714 039	0.0608	− 19.64	11.37	S	0.31	0.09	2.23 ± 0.23
1-229010	57.243 038	− 1.144 831	0.0407	− 20.51	11.46	–	0.41	0.03	2.11 ± 0.09
1-211311	248.426 392	39.185 120	0.0298	− 19.04	10.44	E/S	0.43	0.02	1.99 ± 0.06
1-373161	222.810 074	30.692 245	0.0547	− 21.30	11.60	E	0.43	0.00	1.87 ± 0.11
1-210646	245.157 181	41.466 873	0.0606	− 20.38	10.98	S	0.18	0.05	1.80 ± 0.10
1-351790	121.147 926	50.708 557	0.0227	− 18.09	9.92	E	0.39	0.02	1.72 ± 0.03
1-163831	118.627 846	25.815 987	0.0631	− 20.84	11.26	S	0.27	0.05	1.67 ± 0.13
1-22301	253.405 563	63.031 269	0.1052	− 21.19	11.18	S	0.29	0.08	1.67 ± 0.23
1-248420	241.823 395	41.403 603	0.0346	− 19.71	10.90	S	0.21	0.07	1.66 ± 0.06
1-23979	258.158 752	57.322 422	0.0266	− 18.27	10.42	E	0.44	0.06	1.60 ± 0.05
1-542318	245.248 306	49.001 778	0.0582	− 19.75	10.91	E	0.34	0.01	1.58 ± 0.07
1-95092	250.846 420	39.806 461	0.0302	− 19.95	11.20	E	0.47	0.04	1.54 ± 0.07
1-279676	173.981 888	48.021 458	0.0587	− 19.40	10.81	–	0.32	0.02	1.52 ± 0.14
1-201561	118.053 215	28.772 579	0.0637	− 19.73	10.88	S	0.30	0.07	1.37 ± 0.15
1-198182	224.749 649	48.409 855	0.0359	− 20.22	11.09	E	0.49	0.01	1.34 ± 0.11
1-96075	253.946 381	39.310 535	0.0631	− 21.12	11.35	S	0.29	0.07	1.26 ± 0.13
1-519742	206.612 457	22.076 742	0.0276	− 17.62	9.64	S	0.23	0.04	1.19 ± 0.03
1-491229	172.607 544	22.216 530	0.0393	− 20.25	11.12	E	0.51	0.02	1.14 ± 0.11
1-604761	113.472 275	37.025 906	0.0618	− 20.92	11.34	S	0.26	0.12	1.00 ± 0.13
1-25725	262.996 735	59.971 638	0.0291	− 18.30	10.55	E	0.44	0.04	0.92 ± 0.05
1-94604	251.335 938	42.757 790	0.0493	− 19.44	10.52	S	0.37	0.01	0.86 ± 0.07
1-37036	41.699 909	0.421 577	0.0283	− 19.02	10.66	E	0.40	0.09	0.84 ± 0.06
1-167688	155.885 559	46.057 755	0.0258	− 17.86	9.75	E	0.52	0.04	0.84 ± 0.02
1-279666	173.911 240	47.515 518	0.0455	− 18.83	10.42	E	0.31	0.02	0.84 ± 0.07
1-339163	116.280 205	46.072 422	0.0312	− 20.02	10.97	S	0.30	0.10	0.82 ± 0.07
1-258774	186.400 864	45.083 858	0.0384	− 19.60	10.77	–	0.55	0.03	0.77 ± 0.10
1-198153	224.289 078	48.633 968	0.0354	− 19.83	11.00	S	0.27	0.07	0.76 ± 0.08
1-91016	234.810 974	56.670 856	0.0463	− 18.60	10.56	S	0.27	0.06	0.76 ± 0.09
1-279073	170.588 150	46.430 504	0.0323	− 19.53	10.79	E	0.51	0.01	0.63 ± 0.06
1-135044	247.907 990	41.493 645	0.0303	− 19.76	10.65	S	0.31	0.05	0.61 ± 0.04

Table 1 – *continued*

mangaID (1)	RA (2)	Dec. (3)	z (4)	M_r (5)	$\log M^\star/M_\odot$ (6)	$GZ1_c$ (7)	C (8)	A (9)	$L([O\,III])$ (10)
1-148068	156.805 679	48.244 793	0.0610	− 20.72	11.41	S	0.22	0.04	0.45 ± 0.15
1-277552	167.034 561	45.984 623	0.0362	− 19.72	10.83	S	0.21	0.15	0.44 ± 0.05
1-217050	136.719 986	41.408 253	0.0274	− 19.66	10.93	E	0.47	0.02	0.43 ± 0.03
1-25554	262.486 053	58.397 408	0.0268	− 19.27	10.52	S	0.36	0.04	0.24 ± 0.03
1-135285	247.216 949	42.812 012	0.0316	− 19.66	10.78	–	0.32	0.05	0.20 ± 0.04

SDSS-III integrated nuclear spectrum, from Thomas et al. (2013). The criterion we have applied to identify galaxies hosting AGN was that it must be located, within the uncertainties, simultaneously in the Seyfert or LINER region of both the BPT and the WHAN diagrams. This criterion eliminates from the sample potential LIERs, and also transition objects. Only 62 galaxies have fulfilled this criterion.

Figs 2 (a) and (b) present the BPT and WHAN diagrams for all MPL-5 emission-line galaxies and indicate the location of galaxies, we have considered as AGN hosts following the criteria above. Table 1 lists relevant parameters of the AGN host galaxies. Besides identifications and coordinates, redshifts, absolute r magnitudes and stellar masses, we also list the galaxy classification in Galaxy Zoo (GZ1, Lintott et al. 2011), the r-band concentration index C and asymmetry parameter A (described below) and the [O III] λ5007 luminosity derived from SDSS-III data (Thomas et al. 2013).

In order to assess quantitatively the morphological variety of the AGN and control samples, we have derived the concentration index C and asymmetry index A of the sample galaxies using the publicly available code PYCA (Menanteau et al. 2005). This calculation was made using the r-band images in order to maximize the galaxy signal-to-noise ratio. We have also obtained for all galaxies of the sample the morphological classifications from GZ1 (Lintott et al. 2011). From the GZ1 classification probabilities, we have separated the galaxies in four large classes: ellipticals (E), spirals (S), merging (M) and intermediate elliptical/spiral (E/S); this last class corresponds to galaxies whose GZ1 elliptical and spiral probabilities are rigorously the same and exceed 50 per cent when combined.

Most of the 62 AGN in our sample have luminosities $L([O\,III]) < 3.8 \times 10^{40}$ erg s^{-1}, with only 17 having larger luminosities. We use this threshold – postulated by Kauffmann et al. (2003) – to characterize these 17 AGNs as 'strong AGN'. SDSS-III *ugriz* negative images (Fukugita et al. 1996) of the four most luminous of these strong AGNs are shown in Fig. 1; the remainder are available online.

Inspection of the SDSS-III spectra showed that most of the strong AGN in our sample present coronal lines: at least one of the lines [NeV] λ3425 Å, [FeV II] λ3760 Å or [FeX] λ6374 Å are detectable above 3σ. A small number of objects among the most [O III]-luminous 'weak AGN' also present some of these lines. Coronal lines are thought to be produced by photoionization from the AGN (Mazzalay, Rodríguez-Ardila & Komossa 2010; Rodríguez-Ardila et al. 2011) and to be associated with outflows (Müller-Sánchez et al. 2011). Being insensitive to star formation as opposed to the [O III] λ5007 Å, the presence of coronal lines reinforces the AGN nature of the 17 most [O III]-luminous objects in our sample, and suggests a transition between high- and low-ionization AGN at $L([O\,III]) = 3.8 \times 10^{40}$ erg s^{-1}, in concordance with Kauffmann et al. (2003).

We note that our AGN selection is based on single-fibre SDSS-III observations, which limits us to sources with AGN-photoionization signatures within 3 arcsec of the galactic centre. Wylezalek et al. (in preparation) has recently developed an AGN selection algorithm taking full advantage of the spatial dimension of AGN ionization signatures provided through the MaNGA data. Wylezalek et al. (in preparation) show that about a third to a half of the MaNGA-selected AGN candidates would not have been selected based on the SDSS-III single-fibre observations since AGN ionization signatures are only prevalent beyond the 3 arcsec coverage of the single-fibre spectra. Reasons for this can be manyfold (off-nuclear AGN, star formation signatures dominate in the centre due to a nuclear starburst, recently turned-off AGN) and are currently under investigation by Wylezalek et al. (in preparation).

In this paper, we focus on the classical AGN with nuclear photoionization signatures. In a forthcoming paper, we will also investigate the nature of the stellar populations in the 'unusual' off-nuclear MaNGA-selected AGN candidates.

2.2 Control sample

We have extracted from MPL-5 a control sample of galaxies with properties matched to those of the AGN hosts, except that their nuclei are quiescent. The control sample was built as follows:

(i) First, we selected from MPL-5 all galaxies, presenting or not detectable emission lines, whose ionizing source is not an AGN (as discussed in Section 2.1). We therefore consider a galaxy as a potential control sample candidate if it fulfills any one of these four conditions: (a) it is located, within the uncertainties, in the star-forming region of the BPT diagram; (b) it is located, within the uncertainties, in the transition or LINER region of the BPT, but the WHAN diagram discards ionization from an AGN based on the value of EWHα; (c) it presents a very large uncertainty in $\log$ [O III]/Hβ, not allowing for a secure classification in the BPT diagram, but the WHAN diagram discards ionization from an AGN based on the value of EWHα; (d) the galaxy does not present emission lines. These conditions make sure that galaxies with prominent emission lines are dominated by star formation, not by an active nucleus; the remaining objects are galaxies whose emission lines can be completely accounted for by hot evolved low-mass stars. Galaxies which fulfill any one of these conditions are considered inactive.

(ii) We have then selected two control galaxies for each AGN, matching then according to the redshift z and total stellar mass $M_\star$. A preliminary list of control sample candidates was drawn for each galaxy in the AGN sample by exploring the full (z, $M_\star$) parameter space for all inactive galaxies in MPL-5. Galaxies for which both z and $M_\star$ did not differ by more than 30 per cent from those of the AGN sample values were visually inspected, allowing for a large number of control objects to be selected while keeping low the dispersion of values in the parameter space. The number of control sample candidates selected at this point for each galaxy was typically ≈ 50 (with a larger/smaller number of candidates for galaxies at low/high redshift).

Table 2. Control sample parameters. (1) identification of the AGN host associated with the control galaxy; (2)–(12) same as (1)–(11) of Table 1. Twelve control sample objects have been paired to more than one AGN hosts and appear more than once in the table.

AGN mangaID (1)	mangaID (2)	RA (3)	Dec. (4)	z (5)	M_r (6)	$\log M^{\star}/M_{\odot}$ (7)	$GZ1_c$ (8)	C (9)	A (10)	$L([O\,III])$ (11)
1-558912	1-71481	117.456 001	34.883 911	0.1312	− 20.95	11.70	E	0.47	0.02	0.10 ± 0.20
	1-72928	127.256 485	45.016 773	0.1270	− 20.62	11.52	E	0.40	0.21	0.09 ± 0.23
1-269632	1-210700	248.140 564	39.131 020	0.1303	− 20.96	11.67	S	0.36	0.03	1.55 ± 0.44
	1-378795	118.925 613	50.172 771	0.0967	− 20.77	11.35	S	0.32	0.03	0.72 ± 0.31
1-258599	1-93876	246.942 947	44.177 521	0.1394	− 20.75	11.50	E	0.44	0.01	0.46 ± 0.36
	1-166691	146.047 348	42.900 040	0.1052	− 20.50	11.36	E	0.51	0.04	0.09 ± 0.49
1-72322	1-121717	118.803 429	35.596 798	0.1098	− 21.11	11.61	S	0.39	0.12	1.40 ± 0.57
	1-43721	116.967 567	43.383 499	0.1114	− 21.41	11.86	S	0.32	0.01	1.91 ± 0.52
1-121532	1-218427	124.342 316	27.796 206	0.1496	− 21.30	11.47	E	0.47	0.04	0.72 ± 0.62
	1-177493	257.085 754	31.746 916	0.1081	− 20.90	11.30	E	0.38	0.06	2.29 ± 0.28
1-209980	1-295095	248.348 663	24.776 577	0.0410	− 18.40	10.14	E	0.35	0.05	0.15 ± 0.03
	1-92626	241.799 545	48.572 563	0.0434	− 20.04	11.04	S	0.36	0.03	0.76 ± 0.07
1-44379	1-211082	247.620 041	39.626 045	0.0304	− 19.72	11.07	E	0.31	0.06	0.19 ± 0.04
	1-135371	250.156 235	39.221 634	0.0352	− 19.20	10.76	S	0.28	0.11	0.25 ± 0.07
1-149211	1-377321	110.556 152	42.183 643	0.0444	− 19.02	9.89	S	0.31	0.03	4.53 ± 0.13
	1-491233	172.563 995	22.992 010	0.0332	− 18.39	10.59	S	0.29	0.06	0.25 ± 0.03
1-173958	1-247456	232.823 196	45.416 538	0.0705	− 20.05	10.83	–	0.40	0.02	0.57 ± 0.16
	1-24246	264.840 790	56.567 070	0.0818	− 19.91	10.57	S	0.75	0.36	0.11 ± 0.06
1-338922	1-286804	211.904 861	44.482 269	0.1429	− 20.03	10.50	M	0.44	0.32	2.23 ± 0.43
	1-109493	56.425 140	− 0.378 460	0.1093	− 20.46	11.26	–	0.49	− 0.01	0.15 ± 0.18
1-279147	1-283246	191.078 873	46.407 131	0.0496	− 19.17	10.55	S	0.47	0.04	0.23 ± 0.06
	1-351538	119.145 126	47.563 850	0.0692	− 19.67	11.00	S	0.35	0.08	0.46 ± 0.13
1-460812	1-270160	248.274 612	26.211 815	0.0660	− 20.37	11.46	S	0.50	0.02	0.70 ± 0.39
	1-258455	183.612 198	45.195 454	0.0653	− 20.02	11.03	E	0.40	0.03	0.49 ± 0.14
1-92866	1-94514	248.241 180	42.524 670	0.0614	− 20.60	11.17	E	0.51	0.00	–-
	1-210614	244.501 755	41.392 189	0.0612	− 20.64	11.48	E	0.49	0.01	0.40 ± 0.14
1-94784	1-211063	247.058 411	40.313 835	0.0331	− 19.87	10.79	S	0.33	0.09	0.20 ± 0.04
	1-135502	247.764 175	39.838 505	0.0305	− 19.51	11.13	S	0.40	0.09	0.50 ± 0.05
1-44303	1-339028	116.097 923	44.527 740	0.0497	− 20.01	11.24	S	0.36	0.06	0.44 ± 0.08
	1-379087	119.910 118	51.792 362	0.0534	− 19.60	11.02	S	0.38	0.10	0.72 ± 0.13
1-339094	1-274646	158.017 029	43.859 268	0.0284	− 18.70	10.36	E	0.53	0.02	0.35 ± 0.04
	1-24099	258.027 618	57.504 009	0.0282	− 18.67	10.34	E	0.44	0.01	0.06 ± 0.03
1-137883	1-178838	312.023 621	0.068 841	0.0247	− 17.54	10.46	–	0.51	0.19	0.10 ± 0.02
	1-36878	42.542 126	− 0.867 116	0.0232	− 18.88	10.77	E	0.45	0.07	0.28 ± 0.04
1-48116	1-386452	136.228 333	28.384 314	0.0269	− 19.54	10.57	S	0.49	0.09	0.32 ± 0.04
	1-24416	263.033 173	56.878 746	0.0281	− 19.16	10.66	S	0.37	0.03	0.22 ± 0.03
1-256446	1-322671	235.797 028	39.238 773	0.0637	− 19.77	10.82	E	0.49	0.04	–-
	1-256465	166.752 243	43.089 901	0.0575	− 19.70	10.79	E	0.50	0.01	0.59 ± 0.11
1-95585	1-166947	147.335 007	43.442 989	0.0720	− 20.79	10.81	S	0.29	0.02	0.13 ± 0.08
	1-210593	244.419 754	41.899 155	0.0605	− 19.76	10.90	S	0.36	0.06	0.43 ± 0.14
1-135641	1-635503	318.990 448	9.543 076	0.0293	− 19.37	10.91	S	0.22	0.10	0.15 ± 0.06
	1-235398	213.149 185	47.253 059	0.0281	− 18.91	10.99	S	0.28	0.10	0.16 ± 0.05
1-259142	1-55572	133.121 307	56.112 690	0.0454	− 20.11	11.03	S	0.40	0.06	0.12 ± 0.04
	1-489649	171.954 834	21.386 103	0.0406	− 19.94	10.95	S	0.40	0.03	0.30 ± 0.08
1-109056	1-73005	125.402 306	45.585 476	0.0514	− 19.47	10.65	S	0.31	0.05	0.20 ± 0.06
	1-43009	113.553 879	39.076 836	0.0510	− 19.41	10.43	S	0.26	0.03	0.12 ± 0.04
1-24148	1-285031	198.701 370	47.351 547	0.0303	− 18.47	10.72	S	0.34	0.05	0.26 ± 0.04
	1-236099	225.236 221	41.566 265	0.0205	− 17.36	9.91	S	0.33	0.04	0.07 ± 0.01
1-166919	12-129446	203.943 542	26.101 791	0.0670	− 20.57	11.32	S	0.34	0.03	0.28 ± 0.09
	1-90849	237.582 748	56.131 981	0.0661	− 20.39	11.16	E	0.30	0.04	0.28 ± 0.05
1-248389	1-94554	248.914 688	42.461 296	0.0318	− 18.96	10.57	S	0.55	0.07	0.22 ± 0.04
	1-245774	214.863 297	54.100 300	0.0426	− 20.22	10.83	S	0.40	0.08	0.29 ± 0.07
1-321739	1-247417	233.319 382	45.698 528	0.0294	− 19.25	10.76	S	0.28	0.09	0.16 ± 0.04
	1-633994	247.419 952	40.686 954	0.0305	− 18.27	11.04	S	0.39	0.11	0.36 ± 0.09
1-234618	1-282144	184.592 514	46.155 350	0.0492	− 18.92	10.31	S	0.21	0.08	0.10 ± 0.02
	1-339125	117.739 944	45.989 529	0.0534	− 18.97	11.17	S	0.35	0.05	0.45 ± 0.23
1-229010	1-210962	246.358719	39.870 697	0.0290	− 20.49	11.09	S	0.47	0.07	0.35 ± 0.06
	1-613211	167.861847	22.970 764	0.0323	− 19.87	11.32	E	0.48	0.04	0.16 ± 0.06

Table 2 – *continued*

AGN mangaID (1)	mangaID (2)	RA (3)	Dec. (4)	z (5)	M_r (6)	$\log M^\star/M_\odot$ (7)	$GZ1_c$ (8)	C (9)	A (10)	$L([O\,III])$ (11)
1-211311	1-25688	261.284 851	58.764 687	0.0292	− 18.79	10.32	S	0.29	0.06	0.10 ± 0.02
	1-94422	250.453 201	41.818 737	0.0316	− 19.15	10.55	S	0.37	0.05	0.24 ± 0.03
1-373161	1-259650	196.611 053	45.289 001	0.0509	− 21.07	11.68	E	0.44	0.06	0.67 ± 0.20
	1-289865	322.048 584	0.299 885	0.0525	− 20.90	11.35	–	0.49	0.02	0.11 ± 0.09
1-210646	1-114306	323.742 737	11.296 529	0.0637	− 20.58	10.83	S	0.26	0.05	0.33 ± 0.16
	1-487130	164.447 296	21.233 431	0.0587	− 20.47	10.86	S	0.26	0.11	0.27 ± 0.10
1-351790	1-23731	260.746 704	60.559 292	0.0205	− 18.20	10.19	E	0.40	0.02	0.02 ± 0.01
	1-167334	151.894 836	46.093 983	0.0243	− 18.89	10.60	E	0.43	0.04	0.47 ± 0.05
1-163831	1-247456	232.823 196	45.416 538	0.0705	− 20.05	10.83	–	0.40	0.02	0.57 ± 0.16
	1-210593	244.419 754	41.899 155	0.0605	− 19.76	10.90	S	0.36	0.06	0.43 ± 0.14
1-22301	1-251871	214.506 760	41.827 644	0.1027	− 21.17	11.68	S	0.26	0.05	0.24 ± 0.18
	1-72914	127.580 818	45.075 867	0.0970	− 20.88	11.31	S	0.23	0.08	0.13 ± 0.07
1-248420	1-211063	247.058 411	40.313 835	0.0331	− 19.87	10.79	S	0.33	0.09	0.20 ± 0.04
	1-211074	247.462 692	39.766 510	0.0318	− 19.71	10.79	S	0.30	0.18	0.20 ± 0.04
1-23979	1-320681	213.813 095	47.873 344	0.0279	− 18.76	10.77	E	0.48	0.01	0.09 ± 0.07
	1-519738	206.514 709	22.118 843	0.0277	− 19.49	10.73	E	0.45	0.03	0.11 ± 0.04
1-542318	1-285052	199.061 493	47.599 365	0.0573	− 19.77	10.85	S	0.32	0.04	0.11 ± 0.03
	1-377125	112.221 359	41.307 812	0.0585	− 19.67	10.84	S	0.41	0.02	0.57 ± 0.14
1-95092	1-210962	246.358 719	39.870 697	0.0290	− 20.49	11.09	S	0.47	0.07	0.35 ± 0.06
	1-251279	209.251 984	43.362 034	0.0329	− 20.11	10.97	E	0.47	0.04	0.37 ± 0.06
1-279676	1-44789	120.890 366	47.892 406	0.0586	− 19.33	10.92	–	0.31	0.13	0.32 ± 0.09
	1-378401	117.904 335	48.000 526	0.0612	− 19.65	11.02	E	0.41	0.02	0.57 ± 0.14
1-201561	1-24246	264.840 790	56.567 070	0.0818	− 19.91	10.57	S	0.75	0.36	0.11 ± 0.06
	1-285052	199.061 493	47.599 365	0.0573	− 19.77	10.85	S	0.32	0.04	0.11 ± 0.03
1-198182	1-256185	165.568 695	44.271 709	0.0370	− 20.00	11.03	E	0.50	0.06	0.25 ± 0.04
	1-48053	132.595 016	55.378 742	0.0308	− 20.24	11.49	E	0.50	0.01	–-
1-96075	1-166947	147.335 007	43.442 989	0.0720	− 20.79	10.81	S	0.29	0.02	0.13 ± 0.08
	1-52259	59.411 037	− 6.274 680	0.0678	− 20.69	11.12	S	0.23	0.07	0.30 ± 0.09
1-519742	1-37079	42.092 335	0.986 465	0.0274	− 17.25	9.55	E	0.27	0.02	0.02 ± 0.01
	1-276679	161.272 629	44.054 291	0.0253	− 18.27	10.10	S	0.24	0.03	0.05 ± 0.01
1-491229	1-94554	248.914 688	42.461 296	0.0318	− 18.96	10.57	S	0.55	0.07	0.22 ± 0.04
	1-604048	50.536 137	− 0.836 265	0.0365	− 20.37	10.91	S	0.42	0.09	0.39 ± 0.08
1-604761	1-210173	241.341 766	42.488 312	0.0778	− 20.71	11.10	S	0.33	0.07	0.52 ± 0.13
	1-71525	118.344 856	36.274 380	0.0457	− 20.17	10.97	S	0.27	0.10	0.19 ± 0.06
1-25725	1-211079	247.438 034	39.810 539	0.0304	− 18.97	10.54	E	0.54	0.01	0.03 ± 0.04
	1-322074	228.700 729	43.665 970	0.0274	− 18.15	10.10	E	0.45	0.02	–-
1-94604	1-295095	248.348 663	24.776 577	0.0410	− 18.40	10.14	E	0.35	0.05	0.15 ± 0.03
	1-134239	241.416 443	46.846 561	0.0571	− 19.83	10.70	S	0.36	0.04	0.23 ± 0.06
1-37036	1-210785	246.765 076	39.527 386	0.0338	− 20.22	10.97	E	0.47	0.01	–-
	1-25680	261.968 872	60.097 275	0.0278	− 19.41	10.84	E	0.52	0.02	0.34 ± 0.04
1-167688	1-235587	214.854 660	45.864 250	0.0267	− 18.88	10.48	E	0.44	0.01	0.08 ± 0.02
	1-37062	41.846 367	0.058 757	0.0248	− 18.30	10.40	E	0.49	0.03	0.27 ± 0.03
1-279666	1-392976	156.428 894	37.497 524	0.0432	− 17.91	10.09	E	0.37	0.02	0.10 ± 0.03
	1-47499	132.037 582	54.309 921	0.0461	− 18.53	10.51	E	0.27	0.04	0.15 ± 0.06
1-339163	1-136125	254.044 144	34.836 521	0.0316	− 19.33	10.50	S	0.25	0.09	0.08 ± 0.02
	1-626830	204.683 838	26.328 539	0.0282	− 19.23	10.67	S	0.28	0.07	0.15 ± 0.04
1-258774	1-379660	119.973 717	55.374 817	0.0357	− 19.44	10.74	E	0.47	0.03	0.37 ± 0.07
	1-48208	134.008 118	57.390 965	0.0406	− 19.57	10.85	S	0.50	0.01	0.12 ± 0.04
1-198153	1-211063	247.058 411	40.313 835	0.0331	− 19.87	10.79	S	0.33	0.09	0.20 ± 0.04
	1-135810	250.123 138	39.235 115	0.0297	− 19.38	10.59	S	0.24	0.09	0.08 ± 0.02
1-91016	1-338828	115.641 609	44.215 858	0.0418	− 18.10	10.42	S	0.28	0.03	0.43 ± 0.05
	1-386695	137.983 505	27.899 269	0.0474	− 19.33	10.48	S	0.27	0.09	0.81 ± 0.09
1-279073	1-211100	247.830 322	39.744 129	0.0309	− 19.15	10.62	E	0.56	0.02	–-
	1-210784	247.097 122	39.570 305	0.0292	− 19.61	10.86	E	0.48	0.00	0.15 ± 0.05
1-135044	1-218280	124.003 311	27.075 895	0.0255	− 19.57	10.81	S	0.27	0.08	0.12 ± 0.03
	1-211063	247.058 411	40.313 835	0.0331	− 19.87	10.79	S	0.33	0.09	0.20 ± 0.04
1-148068	1-166947	147.335 007	43.442 989	0.0720	− 20.79	10.81	S	0.29	0.02	0.13 ± 0.08
	1-55572	133.121 307	56.112 690	0.0454	− 20.11	11.03	S	0.40	0.06	0.12 ± 0.04

Table 2 – *continued*

AGN mangaID (1)	mangaID (2)	RA (3)	Dec. (4)	z (5)	M_r (6)	$\log M^\star/M_\odot$ (7)	$GZ1_c$ (8)	C (9)	A (10)	$L([O\,III])$ (11)
1-277552	1-264513	236.941 513	28.641 697	0.0333	− 20.92	11.28	S	0.25	0.18	0.33 ± 0.05
	1-136125	254.044 144	34.836 521	0.0316	− 19.33	10.50	S	0.25	0.09	0.08 ± 0.02
1-217050	1-135372	250.116 714	39.320 118	0.0301	− 20.29	11.08	E	0.49	0.02	0.01 ± 0.23
	1-274663	157.660 522	44.012 722	0.0280	− 19.88	11.00	E	0.50	0.01	0.08 ± 0.02
1-25554	1-135625	248.507 462	41.347 946	0.0284	− 19.06	10.56	S	0.43	0.05	0.56 ± 0.04
	1-216958	136.200 287	40.591 721	0.0270	− 18.95	10.41	S	0.51	0.03	0.23 ± 0.02
1-135285	1-633990	247.304 123	41.150 871	0.0296	− 19.06	10.46	S	0.34	0.03	0.25 ± 0.03
	1-25688	261.284 851	58.764 687	0.0292	− 18.79	10.32	S	0.29	0.06	0.10 ± 0.02

(iii) The images of the control candidates for each galaxy in the AGN sample were then visually inspected to select control galaxies with similar morphologies and axial ratios to those of the AGN host galaxies. For late-type galaxies, we have tried to reproduce both the structure and development of the arms and the relative bulge size, as well as the line-of-sight orientation and the presence of dust lanes. The priority in the morphological analysis was given to structures closer to the nucleus; i.e. we have assigned more weight to the presence of bars and rings than to the morphology of the arms in the outer galaxy regions. During this step the number of potentially good candidates, i.e. galaxies that are morphologically comparable to the respective AGN host, decreased in many cases to only two galaxies. In order to produce the best statistical comparison with the AGN sample properties, keeping an homogeneous representation of all AGN hosts in the control sample, only the two galaxies that best matched the morphology of the AGN host, according to the above criteria, were chosen for each AGN in the sample.

We have thus produced 124 pairs of AGN and control partners. Twelve of the control sample objects were selected as 'control partners' of two or more AGN hosts simultaneously; therefore, our control sample comprises 109 non-active galaxies, reproducing the distribution of redshift and stellar mass of the AGN sample. Figs 2(c) and (d) present the BPT and WHAN diagrams for the control sample, superimposed on the distribution of the full MPL-5 sample. Six control sample galaxies did not present any emission lines, and thus do not appear in the figures. We can see a bimodal distribution with a clear separation between star-forming galaxies and LIERs. Comparing with the diagrams shown in Figs 2(a) and (b), we can see that AGN and non-AGN have markedly distinct distributions.

3 STELLAR POPULATIONS

In order to characterize the stellar population of the inner 3×3 arcsec^2 of the galaxies, we performed stellar population synthesis using the STARLIGHT code, developed by Cid Fernandes et al. (2005). This code combines, in different proportions, $N_\star$ single stellar populations (SSPs) in order to reproduce a galaxy observed spectrum – excluding emission lines –, O_λ, with a model spectrum, M_λ. Each combination is found by solving the equation

$$M_\lambda = M_{\lambda_0}\left[\sum_{j=1}^{N_\star} x_j b_{j,\lambda} r_\lambda\right] \otimes G(v_\star, \sigma_\star), \quad (1)$$

were $b_{j,\lambda}\, r_\lambda$ is the reddened spectrum of the j-th SSP normalized at λ_0; $r_\lambda = 10^{-0.4(A_\lambda - A_{\lambda 0})}$ is the reddening term; $M_{\lambda 0}$ is the synthetic flux at the normalization wavelength; $\boldsymbol{x}$ is the population vector. The symbol $\otimes$ denotes the convolution operator and $G(v_\star, \sigma_\star)$ is the Gaussian distribution used to model the line-of-sight stellar motions; it is centred at velocity $v_\star$ with dispersion $\sigma_\star$. The reddening law, we have used is that presented by Cardelli, Clayton & Mathis (1989). The adopted normalization wavelength was λ_0 =5700 Å. This wavelength, usually selected to avoid emission and absorption features, is similar to those adopted on other spectral synthesis studies, allowing a comparison of our results with previous ones.

The best-fitting model is determined by minimizing (through a simulated annealing plus Metropolis scheme) the equation

$$\chi^2 = \sum_\lambda [(O_\lambda - M_\lambda) w_\lambda]^2, \quad (2)$$

where emission lines and spurious features are masked by assigning w_λ=0 to these regions.

The spectral basis comprise the 'standard' 45 elements set, which is a sample of the Evolutionary Population Synthesis models presented by Bruzual & Charlot (2003). It covers 15 ages: 0.001, 0.0031, 0.005, 0.01, 0.025, 0.04, 0.10, 0.28, 0.64, 0.94, 1.43, 2.5, 5.0, 11.0 and 13.0 Gyr, and three different metallicities: 0.004, 0.02, 0.05 $Z_\odot$.

Since, we are fitting the spectra of AGN, the signature of the central engine cannot be ignored. This component was represented by a featureless continuum (FC) of power-law form that follows the expression $F_\lambda \propto \lambda^{-0.5}$ (see Koski 1978; Riffel et al. 2009, for example).

3.1 Results for the stellar population

Running the STARLIGHT code allows the measurement of the relative contribution of each SSP vector, characterized by age and metallicity, to the total stellar light at 5700 Å (x_j) and its corresponding contribution to the total stellar mass (μ_j), that are the main quantities required to characterize the star formation history of the centre of these galaxies. The individual contribution of each SSP allows the derivation of the contribution of the main age and metallicity components to the total flux at 5700 Å, although there are other parameters that globally represent the age and metallicity of the stars: the mean light-weighted and mass-weighted ages ($\langle t_L \rangle$ and $\langle t_M \rangle$) and the light-weighted and mass-weighted metallicities ($\langle Z_L \rangle$ and $\langle Z_M \rangle$, Cid Fernandes et al. 2005). The mean age, weighted by light and mass are, respectively, given by

$$\langle t_L \rangle = \sum_{j=1}^{N_\star} x_j \log t_j \quad \langle t_M \rangle = \sum_{j=1}^{N_\star} \mu_j \log t_j, \quad (3)$$

and the mean metallicities, weighted by light and mass, are expressed by

$$\langle Z_L \rangle = \sum_{j=1}^{N_\star} x_j Z_j \quad \langle Z_M \rangle = \sum_{j=1}^{N_\star} \mu_j Z_j, \quad (4)$$

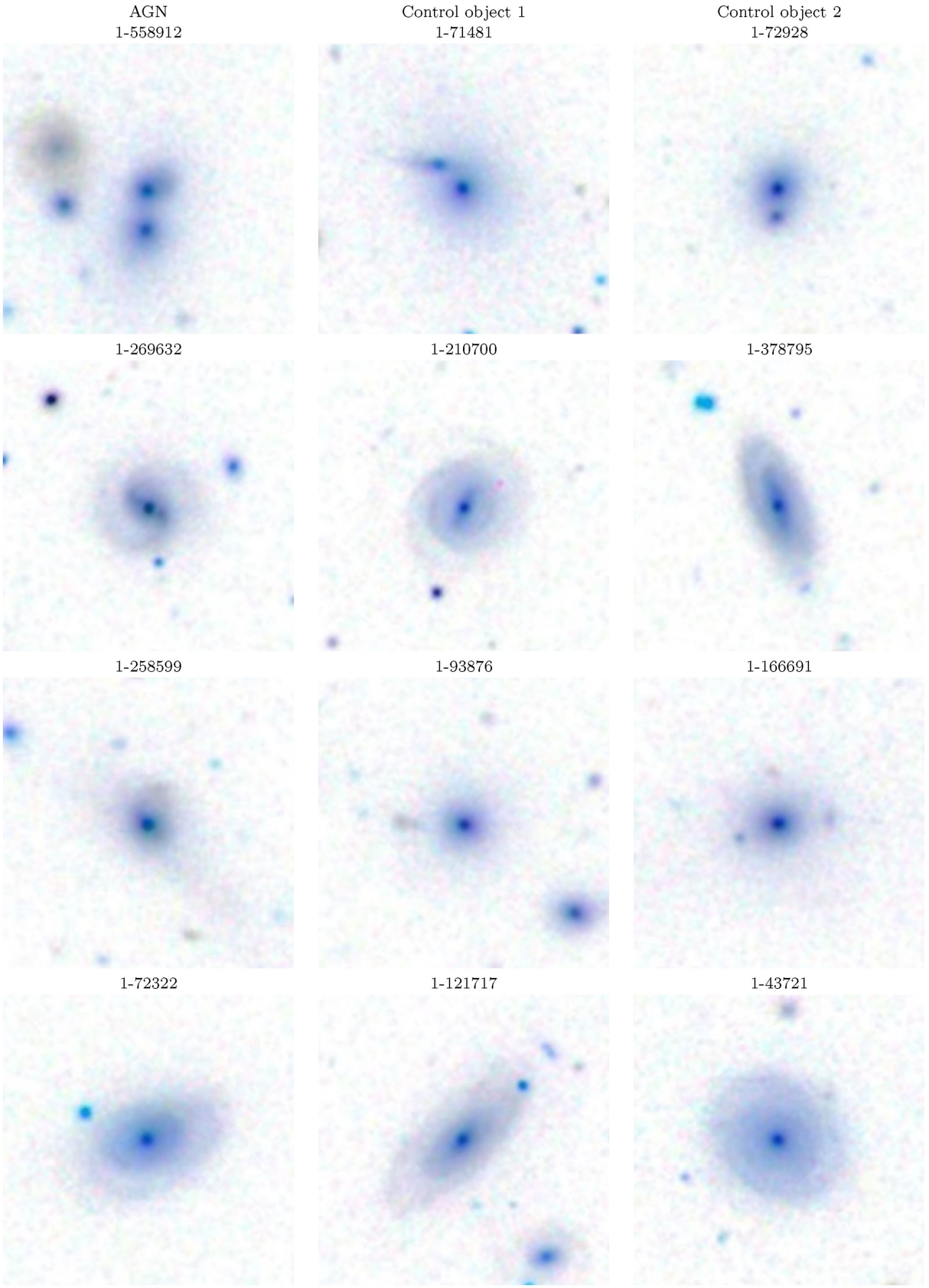

Figure 1. SDSS-III *ugriz* negative images of the four strongest AGN from our sample (left-hand columns) and their control sample equivalents (centre and right-hand columns). The mangaID of each host is indicated above its respective panel. Each chart is 51 arcsec on a side; north is up, east to the left.

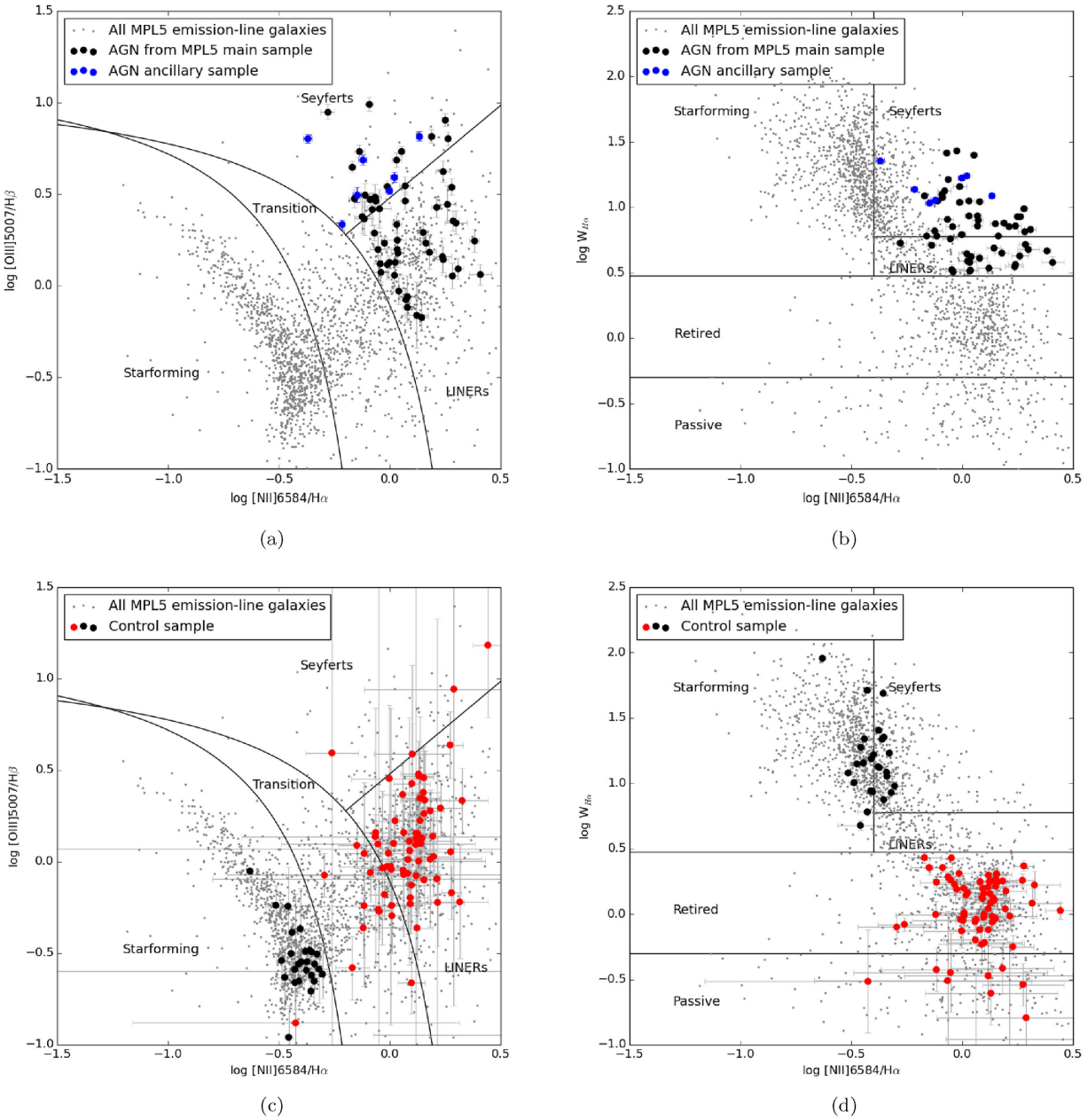

Figure 2. BPT and WHAM diagrams for our sample of confirmed AGN (top panels) and control sample (bottom panels), using the fluxes from Thomas et al. (2013). We only include objects where the emission lines are detected at the 3σ level. The continuous lines separating Seyferts, transition objects, LINERs and star-forming galaxies are from Kauffmann et al. (2003), Kewley et al. (2001) and Cid Fernandes et al. (2010). Grey dots indicate the position of all emission-line galaxies in MPL-5. In the top panels, we indicate as black (blue) circles the confirmed AGN drawn from the MaNGA MPL-5 main sample (AGN Ancillary Sample). In the bottom diagrams, star-forming (retired/passive) control sample objects are represented by black (red) circles. Six objects from the control sample do not present detectable emission lines and are not shown in the diagrams.

respectively.

A strong contribution of one single SP age tends to be spread over different SSP components of similar ages (Cid Fernandes et al. 2001); thus, one must be must be careful interpreting a single SSP component. In order to obtain a more robust and reliable description of the SFH, the SSPs are usually grouped in age bins (e.g. Dametto et al. 2014), which we have chosen as follows: *young–young*: x_{yy} ($t \leq 10 \times 10^6$ yr), *young–old*: x_{yo} ($25 \leq t \leq 40 \times 10^6$ yr), *intermediate–young*: x_{iy} ($0.100 \leq t \leq 0.287 \times 10^9$ yr), *intermediate–intermediate*: x_{ii} ($0.640 \leq t \leq 0.905 \times 10^9$ yr), *intermediate–old*: x_{io} ($1.0 \leq t \leq 2.5 \times 10^9$ yr) and *old*: x_o ($4.0 \leq t \leq 13.1 \times 10^9$ yr).

Fig. 3 presents an example of the results of the stellar population synthesis for the strong AGN mangaID 1-269632. The upper panels show the observed and synthetic spectrum as well as the corresponding residuals; the bottom panels display the resulting light (percent contribution of each age bin above to the light at 5700 Å) and mass contributions of single and binned SSPs vectors. Also shown are the mean ages and metallicities. The inner ∼3.7 kpc of

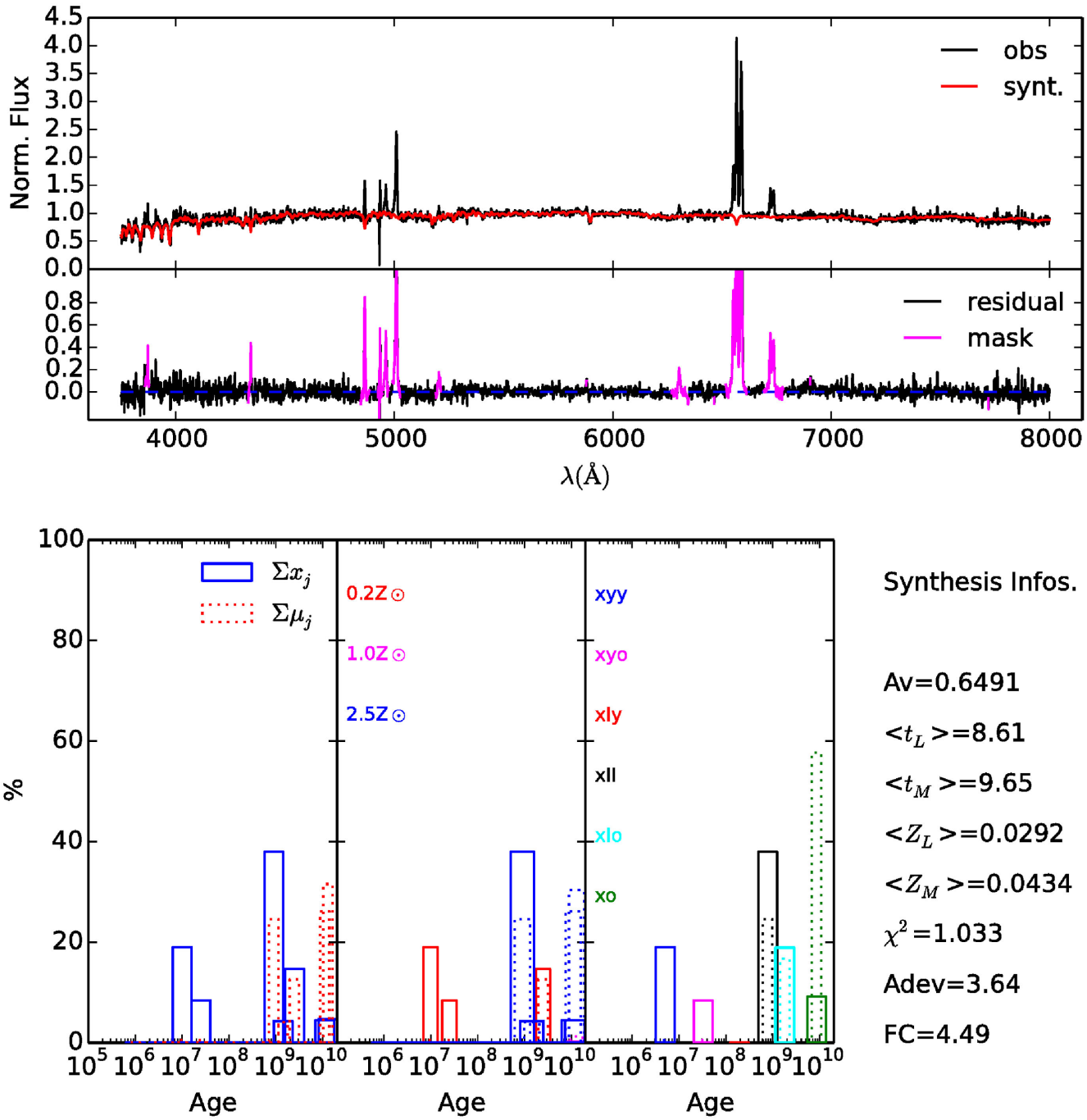

Figure 3. Results from the stellar population synthesis for the strong AGN mangaID 1-269632. Upper two panels: top panel – observed (black) and synthetic (red) spectrum; bottom panel – residuals (observed spectrum - synthetic), with the masked regions highlighted in magenta. Bottom three panels: histograms where solid lines represent the light-weighted contribution of the SSPs and the dashed lines represent the mass-weighted contribution. The left histogram shows the individual contribution of each SSP, sorting the SSP vectors by age and summing the metallicities; the middle histogram displays the same as the left histogram but separating the contribution of each SSP in metallicity, with different colours indicating different metallicities; the right histogram presents the mass contributions of the SSPs divided in six age bins (see the text), and summing the metallicities. To the right and bottom are presented the derived average ages and metallicities (both mass- and light-weighted), the extinction A_V, the contribution of the FC in percent units, the chi-squared value of the fit and the average of the absolute percent difference between observed and synthesized spectra, Adev, that parameterizes the quality of the fit.

this galaxy is dominated by the contribution of intermediate age stars ($x_{ii} \approx 38$ per cent and $x_{io} = 19$ per cent) with old stars contributing $x_o \approx 9$ per cent and young stars $x_{yy} \approx 19$ per cent, which implies that at least one episode of star formation has occurred in the last 10 Myr. Tables with the synthesis results for all galaxies, both for the AGN and control samples, showing the contribution of the six age bins listed above (both in percent flux at 5700 Å and in mass) are presented in the Appendix.

Fig. 6 summarizes the results from the synthesis in histograms of the percent contribution of each age bin to the continuum at 5700 Å.

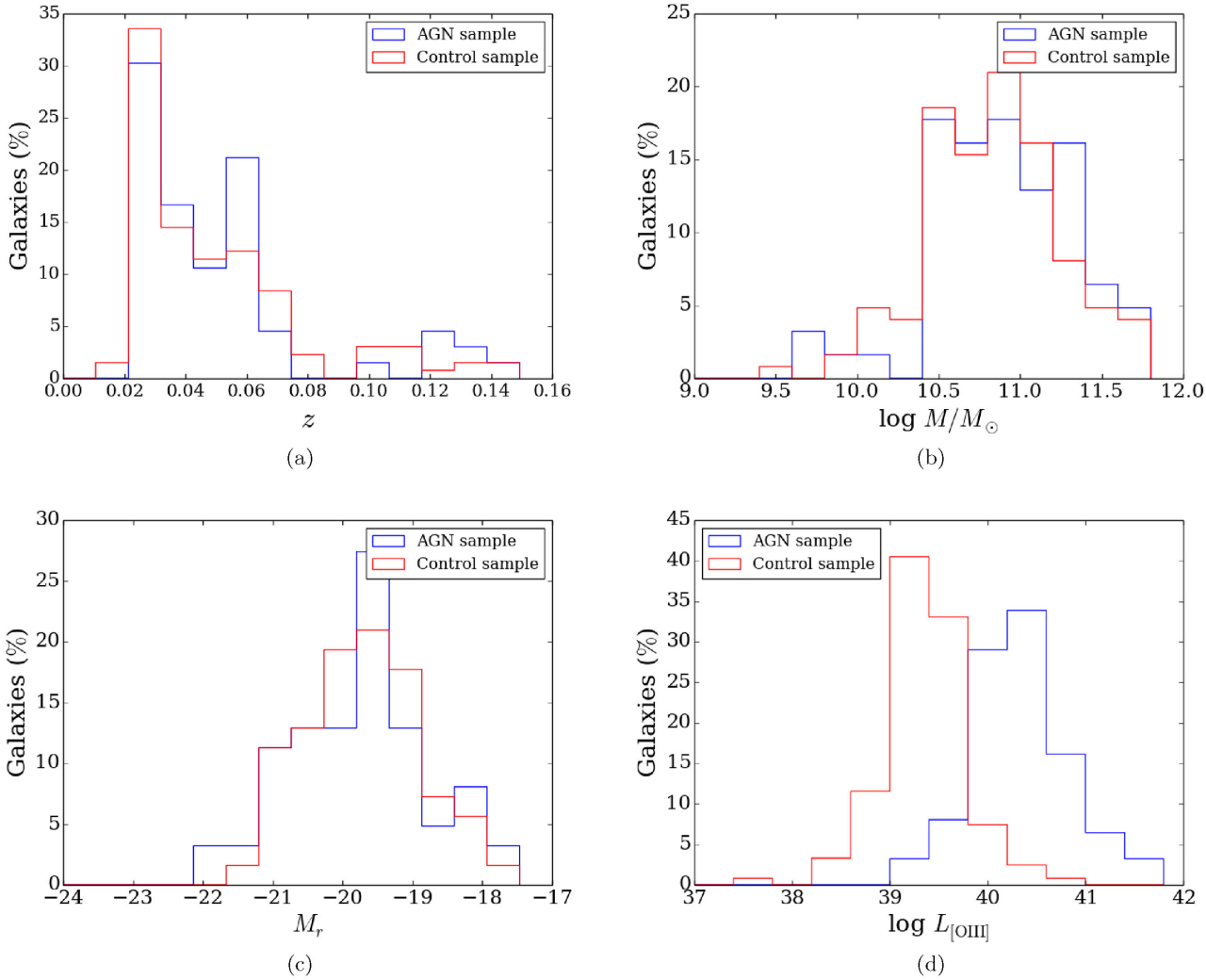

Figure 4. Distributions of redshift (a), stellar mass (b), absolute *r*-band magnitude (c) and [O III] luminosity (d) of the AGN host sample (blue) and the control sample (red). The AGN and the control sample present markedly different distributions of L([O III]), but have the other parameters similar between the two samples.

The results for the AGN sample are shown in blue for the 'weak AGN' (L([O III]) $< 3.8 \times 10^{40}$ erg s^{-1}), in green for the strong AGN and red for the control sample. In these histograms, we have chosen to present the results in bins of 10 per cent for the three oldest age ranges and in bins of 3 per cent for the three youngest ages ranges. We have adopted these smaller bins for the youngest ages to better sample the age distributions, as these ages never contribute more than 30 per cent to the total flux at 5700 Å, allowing us to restrict the *x*-axis to a maximum contribution of 30 per cent.

4 DISCUSSION

4.1 Comparison between the AGN hosts and control sample

After selecting the control sample objects according to the criteria described in Section 2.2, we now check if the resulting distribution of stellar masses and redshifts are indeed compatible with that of the AGN hosts. In Fig. 4, we show the distributions of stellar mass, *r*-band absolute magnitude and redshifts of the AGN sample and the control sample. The distributions of stellar mass and *r*-band absolute magnitude of the two samples are very similar. The probability that these distributions for the AGN and non-AGN galaxies are not drawn from the same distribution is less than 5 per cent as indicated by an Anderson–Darling test (A-D test). Regarding the redshift distribution, the two samples are also similar; the statistical significance of the A-D test is lower (16 per cent), but this is not critical to our analysis. The only significant difference observed in Fig. 4 is for the distribution of the [O III] luminosity L([O III]), as expected: while the centroid of the distribution for the AGN sample is log L([O III]) $\approx$ 40.5, for the control sample the centroid is log L([O III]) $\approx$ 39.3.

We have also made a quantitative assessment of how well the control sample morphological distribution matches that of the AGN hosts. The GZ1 classification reveals that the AGN sample contains 34 (55 per cent) spiral and 18 (29 per cent) elliptical galaxies. The remaining 10 objects (16 per cent) comprise 6 E/S galaxies, 1 merger and 3 unclassified objects. The morphological distribution of the control sample is the same within the uncertainties: 60 per cent spiral and 34 per cent elliptical galaxies. Fig. 5 displays the concentration and asymmetry distributions of the AGN and the control sample galaxies. The dashed line is the optimal separation between the GZ1 major classes (ellipticals and spirals) in the diagram. The

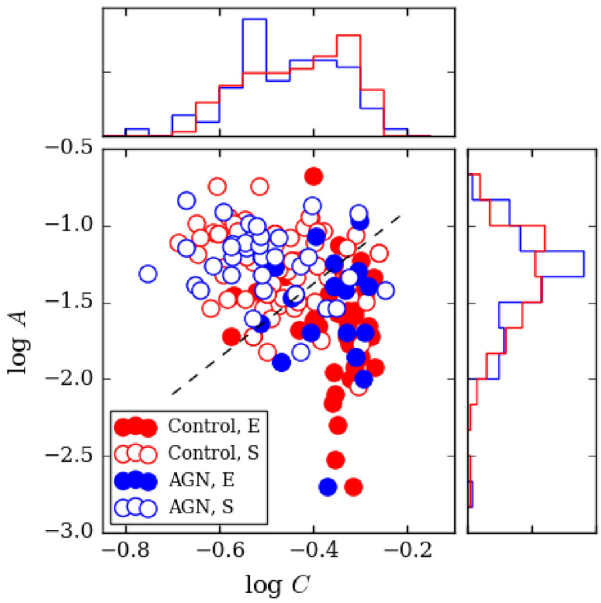

Figure 5. Concentration C and asymmetry A indices values for AGN and the control sample galaxies. The Galaxy Zoo I morphological classification as ellipticals or spirals is represented by filled and open circles, respectively. Blue (red) circles represents AGN (control sample). The dashed line roughly separates the spiral and elliptical-dominated regions in the diagram. The distributions of A and C are similar, but the AGN present a small tendency to be more concentrated near the dashed line.

code PYCA does not calculate uncertainties in C and A, but the good separation between elliptical and spiral galaxies in the C–A plane, with elliptical galaxies occuppying the locus of low asymmetry and high concentration, suggests that the estimates of these parameters are robust. The distributions of AGN hosts and non-active galaxies in the C–A plane are similar, although a small systematic effect is discernible in the sense of a wider distribution of the control sample galaxies in the C–A diagram relative to the AGN. This behaviour is produced by the fact that AGN galaxies appear to be less common in the extremes of low concentration/low asymmetry indices. This result suggests that the AGN sample is morphologically less diverse than the control sample, preferring to populate the intermediate region between ellipticals and spirals. This trend is, however, secondary, as the A-D test results in a p-value larger than 0.2 for the null hypothesis that the C and A distributions for AGN and control sample are drawn from the same distribution.

The combined SDSS-III *ugriz* images of the four strongest AGN from our sample and their 'control partners' are shown in Fig. 1. Those for the rest of the sample are available online. Both figures reveal an apparent very good match in the morphology and axial ratios between the AGN and control sample.

4.2 Stellar population properties

Fig. 6 shows that there is no clear difference between the stellar population of all AGNs – considering both the weak and strong AGNs together – and the control sample. But, when comparing only strong AGN with their control sample, the distributions differ at the 2σ level for x_{yo} and x_o. Though the differences between the distributions are not obvious in these plots due to the histogram binning, they can be seen with smaller bin widths and are confirmed by the results of the A-D tests. The numbers in the top right-hand corners of each panel in Fig. 6 give the probability that the two distributions are derived from the same sample. The small values for x_{yo} and x_o indicate that the contribution of these populations to the light at 5700 Å differ between the strong AGN and the control sample, in the sense that the strong AGN show a smaller contribution from the old stellar population and a larger contribution from the young–old component than the control sample.

The above results suggest that, when comparing weak and strong AGNs, the contribution of old stellar populations decreases, while that of the younger stellar populations increases in the latter. This trend agrees with the previous results by Kauffmann et al. (2003), who compared the stellar population properties of AGN-host galaxies and normal galaxies for a sample of ∼22 600 galaxies with SDSS-I spectra (York et al. 2000). These authors studied the mean stellar age and stellar formation history of these AGN by measuring the indices $D_n(4000) \times W(H\delta)$ (Balogh et al. 1999). They found that weak AGNs have mostly old stellar populations that are similar to those of early-type galaxies (non-AGN), while the strong AGNs have much younger stellar ages and typically strong H δ absorption-line equivalent width, indicating that they have experienced a burst of star formation in the past 1–2 Gyr. Our sample of strong AGN is comprised so far by 17 hosts, but our results are robust, as supported by the A-D tests, and will be increased as more of these objects are observed with MaNGA.

The results of the synthesis for the FC continuum, presented in Fig. 7, show a clear difference between the AGN and control sample: while the control sample tend to show very small contribution of FC in most cases, for the AGN, and in particular for the strong AGN, the FC contribution tends to be larger, as expected. In any case, this contribution is usually smaller than 10 per cent, and in only a few cases it reaches ∼20 per cent. But we also point out that a common problem of stellar population syntheses of the spectra of active galaxies is that a reddened young starburst ($t \leq$5M yr) is very difficult to distinguish from that of an AGN continuum, as discussed in previous studies (Cid Fernandes & Terlevich 1995; Storchi-Bergmann et al. 2000; Cid Fernandes et al. 2004; Riffel at al. 2009). This is particularly true when the FC contribution is smaller than ≈ 20 per cent, as is the case here. We thus conclude that, although some degeneracy may be occurring, the fact that we are finding more FC contribution for the AGN than for the control sample supports that we are being able to separate this contribution in many cases. In order to estimate the impact of this degeneracy on the derived population fractions, we have performed a series of simulations. We have combined a set of SSPs from our base with contributions similar to those we have found of our sample, and added a moderate FC contribution of 10 per cent. We have then perturbed the individual flux values using the same error distribution as the sample spectra, and run STARLIGHT with the same configuration as before, both allowing or not allowing for an FC in the fit. We have found that, when the FC is present but the synthesis does not allow for an FC in the fit, the contributions of young and intermediate stellar populations are overestimated by ∼5 per cent, on average. However, when the FC is allowed, the contribution of young stellar populations is only slightly overestimated (∼2 per cent). This agrees with the recent results of Cardoso, Gomes & Papaderos (2017) that have shown that, for a broad range in star formation histories, the effect of an FC in the derived mean stellar ages is typically lower than 0.1 dex even for FC contributions as large as 40 per cent. Therefore, in the cases that there may be some degeneracy, the effect should be small, with no significant influence on the results of the synthesis discussed above.

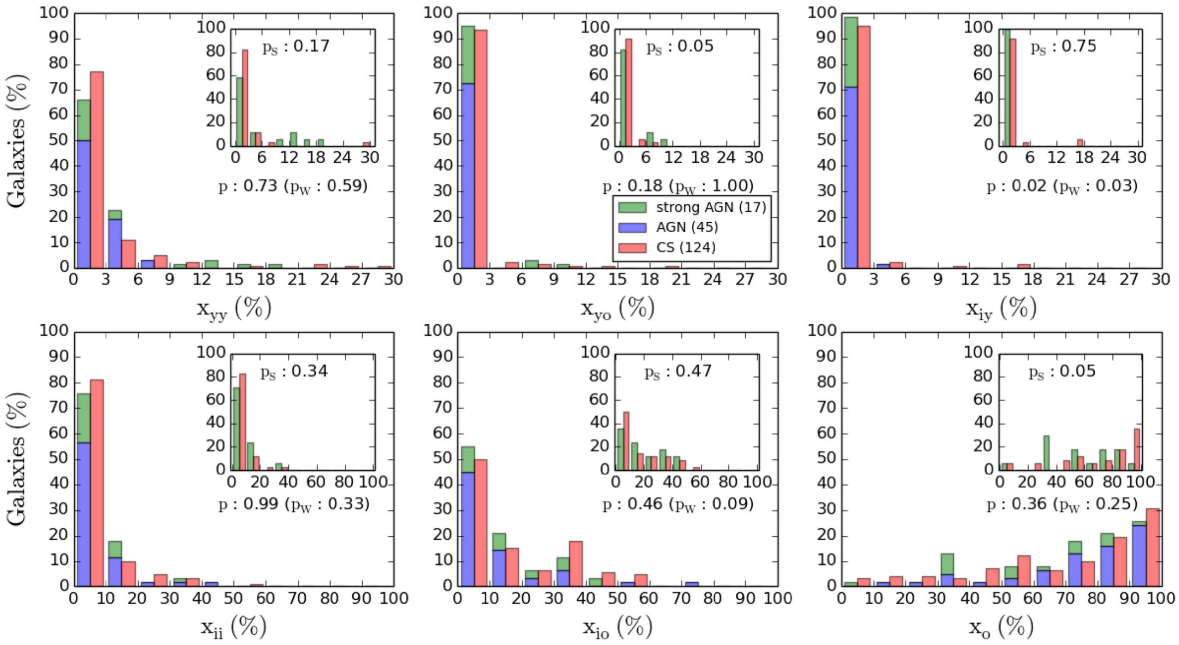

Figure 6. Histograms of the distribution of galaxies according to the fractional contribution of each age bin to the total light at rest frame 5700 Å. Weak AGNs are represented in blue, strong AGNs in green and control sample in red. For the age bins x_{ii}, x_{io} and x_o, we show, in an insert, histograms comparing only the strong AGN (green) with its respective control sample (red). For each histogram, the p-value of the A-D test is given. We also present, below the insert in each plot, the p-value of the comparison between the weak AGN and the control sample. p_w refers to the weak AGN, p_s refer to the strong AGN and p to the combined sample of strong and weak AGNs.

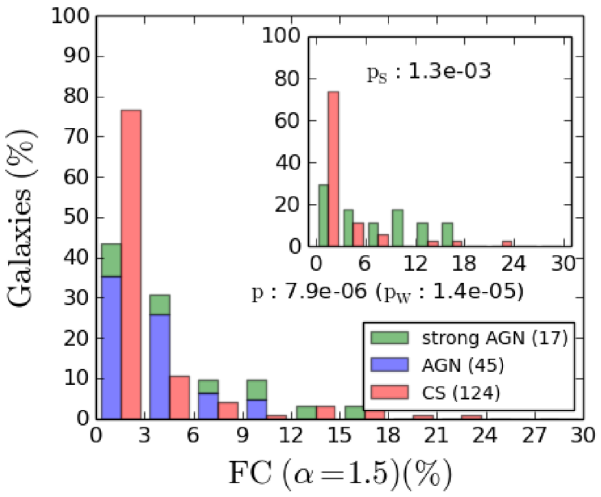

Figure 7. Distribution of galaxies according to the fractional contribution of the FC to the total light at rest frame 5700 Å. Weak AGNs are represented in blue, strong AGN in green and control sample in red. In the insert, we show the histogram comparing only the strong AGN (green) with its respective control sample (red). The p-values of the A-D test of the comparison between the AGN sample and the control sample are also shown. p_w refers to the weak AGN, p_s refer to the strong AGN and p to the combined sample of strong and weak AGNs.

The distribution of the global parameters, mean ages, $\langle t_L \rangle$ and $\langle t_M \rangle$, and mean metallicities, $\langle Z_L \rangle$ and $\langle Z_M \rangle$, are presented in Fig. 8. This figure shows that the distribution of mean ages (weighted in light) differ at the 2σ level between the weak AGN and the control sample, while no such difference is observed for the strong AGN. On the other hand, if one calculates the median age for all weak and all strong AGN, one finds no difference relative to the controls for the weak AGN ($\langle t_L \rangle = 9.90 \pm 0.25$) but a difference of 0.2 dex (younger) for the strong AGN ($\langle t_L \rangle = 9.70 \pm 0.25$, with the controls presenting the same value as observed for the weak AGN).

Regarding the metallicity, Fig. 8 reveals a small difference between the weak AGN and their control sample, with a probability of only about 1 per cent that the distributions are similar in the case of normalization in light (Z_L), while no such difference is observed for the strong AGN. Although the difference in metallicity between the AGN hosts and control galaxies may be due to a different origin for the stars, there is also the possibility that we are observing the effect of degeneracy between age and metallicity in optical spectra (Worthey et al. 1994). This degeneracy arises because the lower metallicity leads to bluer stellar atmospheres, what is also the signature of young stars. As this effect is small, we defer its analysis to a future study, when we have a larger sample of AGN hosts.

4.2.1 The effect of the AGN luminosity

Although we have explored the effect of the AGN luminosity above by separating the analysis of the stellar population in only two populations – strong and weak AGNs – we now investigate in more detail this effect by looking for possible correlations of the stellar population properties with L[O III]. We also take advantage of our careful selection of the control sample to explore the differences between the properties of each AGN host and its two controls, investigating how these differences may be associated with the AGN luminosity.

For this exercise, we calculated the differential fractional contributions (AGN - control): the differences Δx (in each age bin x) of the fractional contributions to the light at 5700 Å between each AGN and its two control partners, and verified how, and if, it depends on the AGN [O III] luminosity. The results are shown in Fig. 9,

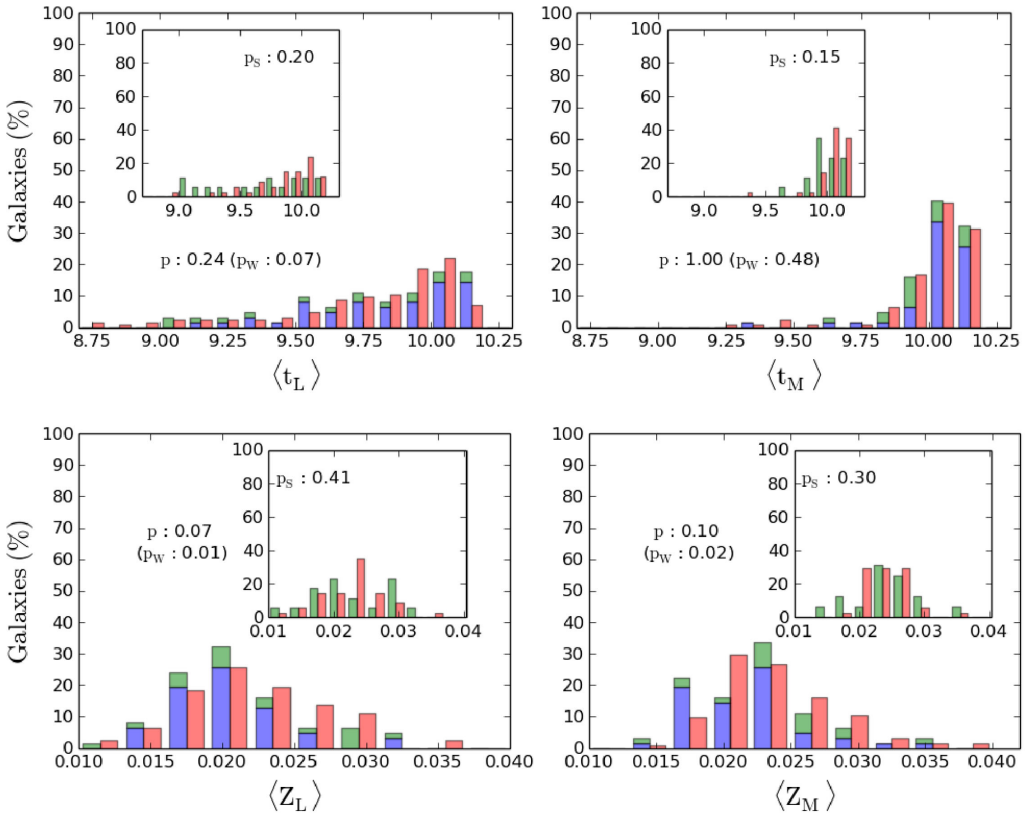

Figure 8. Histograms showing the distributions of the mean ages (top panel) and metallicities (bottom panel), for the AGN (blue for weak and green for strong) and control sample (red). In the insert of each panel, we plot the histograms comparing the strong AGN (green) with its respective control sample (red). For each histogram, the p-value of the A-D test is given. p_w refers to the weak AGN, p_s refer to the strong AGN and p to the combined sample of strong and weak AGNs.

where the limit between strong and weak AGN is shown as a vertical dashed line. We have performed a linear regression between Δx and L[O III] for each age bin and the best fit is shown as a continuous line in the different panels of the figure.

There is an obvious correlation between Δx and L[O III] for some age bins. This is the case for x_{yo}: a Spearman test gives a correlation coefficient of 0.53 with a p-value of 0.0039. For the oldest age bin, x_o, there is an anticorrelation between Δx and L[O III], with a Spearman correlation coefficient of -0.30 and a statistical significance higher than 3σ. Another result from this figure is that an AGN host can have a higher or lower contribution of a given age bin, depending on the AGN luminosity. In the bin x_o, for example, the contribution is higher in lower-luminosity AGN than in their 'control partners', while the opposite is true for luminous AGN, which present a smaller contribution of this age bin than their respective control galaxies. A similar behaviour can be seen in the bin x_{yo}: the relative contribution of this age bin for low-luminosity AGN is smaller, but for high-luminosity AGN is higher.

We have also explored how the differences $\Delta\langle t\rangle$ in the (light-weighted and mass-weighted) logarithmic mean stellar age between AGN and control sample (which we will refer to as 'differential age') depends on the AGN luminosity. The result is shown in Fig. 10. It is evident that $\Delta\langle t\rangle$ and L[O III] show an inverse correlation, especially for the light-weighted mean ages. The resulting Spearman correlation coefficient is -0.27, with a statistical significance higher than 2σ. The overall results agree with those obtained in Fig. 9 and indicate that luminous AGN are younger, on average, than inactive galaxies with similar properties. Low-luminosity AGN, in contrast, present older stellar populations than the control sample. Note, also, that the separation between these two AGN categories is very close to the threshold $L([\mathrm{O\,III}]) = 3.8 \times 10^{40}$ erg s^{-1} (the vertical dashed line), which marks the separation between our weak and strong AGN samples. These results agree with those from Kauffmann et al. (2003), which showed that, at fixed stellar mass density, luminous AGNs present younger stellar populations than inactive galaxies, while low-luminosity AGNs are older, on average.

In order to translate the above results in numbers, we show in Table 3 the mean ages of the AGN and their control galaxies separated in bins of AGN luminosity. Although some bins still have a few galaxies (that we hope to increase as the survey progresses), and the dispersion in the mean age values is large, Table 3 shows a steady decrease of the mean age of the host galaxy as the AGN luminosity increases, besides showing also the trend discussed regarding the difference in age between the AGN hosts and controls.

4.3 Results from MaNGA data

As pointed out in the Introduction, we are applying the same methodology described above to study the resolved stellar population in the MaNGA data (Mallmann et al., in preparation, hereafter Paper II). The SDSS-III spectra correspond to a region of radius 1.5 arcsec around the nucleus – corresponding to a range of radii from ≈ 1 to 3 kpc at the distance of the galaxies. This is similar to the area covered by the central pixel of the MaNGA array. Thus we have checked, for a subsample of representative galaxies, whether

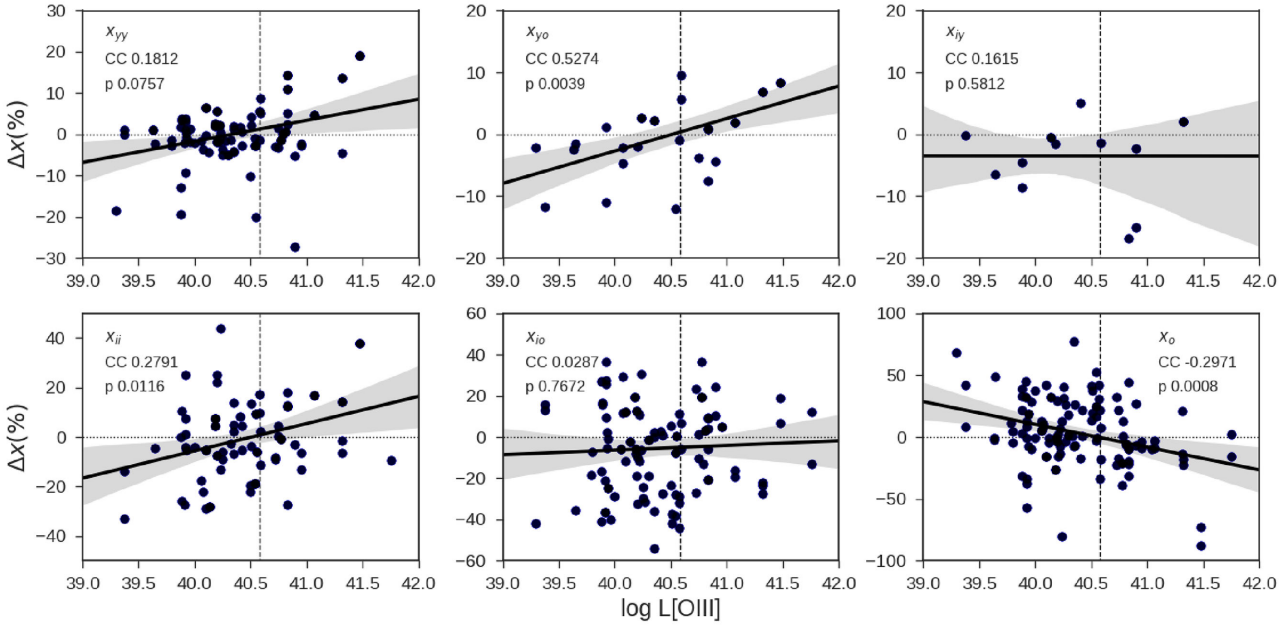

Figure 9. Differences Δx in the fractional contribution of each age bin to the total light at rest frame 5700 Å between AGNs and control galaxies, as a function of the AGN [O III] luminosity. Each circle correspond to a pair AGN/control object. We have excluded pairs for which the fractional contributions are both zero. The best-fitting linear regression and its uncertainties are shown with a thick line and a shaded area, respectively. The Spearman correlation coefficient and the p-value of the test are given in each pannel. The [O III] luminosity that separates strong and weak AGN is shown as a vertical dashed line. The locus $\Delta x = 0$ is shown by a dotted line.

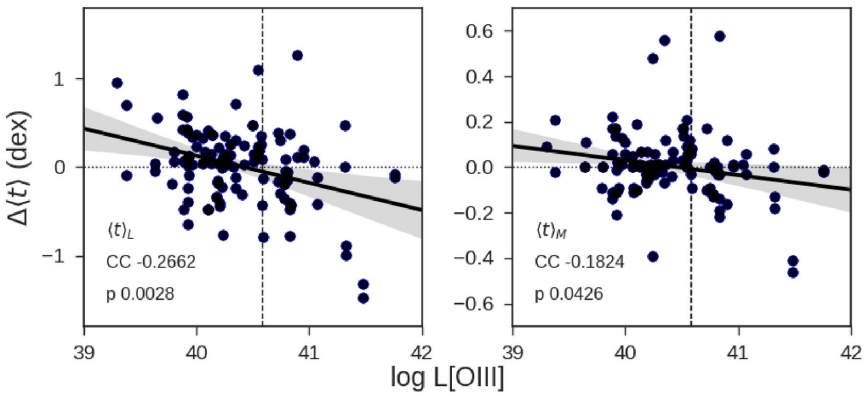

Figure 10. Light-weighted (left-hand panel) and mass-weighted (right-hand panel) differences $\Delta\langle t\rangle$ in the mean stellar age between AGNs and control galaxies, as a function of the AGN [O III] luminosity. The symbols are the same as in Fig. 9.

Table 3. Average of global parameters $\langle t_L\rangle$ and $\langle t_M\rangle$, for the AGN and their control galaxies separated by luminosity.

$\log_{10}$ L[O III] (erg s^{-1})	N (AGN)	Sample	$\langle t\rangle_L$ $\log_{10}$ (yr)	$\Delta\langle t\rangle_L$ dex(yr)	$\langle t\rangle_M$ $\log_{10}$ (yr)	$\Delta\langle t\rangle_M$ dex(yr)
39.0–39.75	5	AGN	9.89 ± 0.16	0.24	10.07 ± 0.03	0.05
		control	9.65 ± 0.42		10.02 ± 0.10	
39.75–40.25	25	AGN	9.81 ± 0.30	0.05	10.00 ± 0.17	0.0
		control	9.76 ± 0.36		10.00 ± 0.19	
40.25–40.75	18	AGN	9.81 ± 0.27	0.10	10.05 ± 0.06	0.04
		control	9.71 ± 0.32		10.01 ± 0.12	
40.75–41.25	10	AGN	9.66 ± 0.35	− 0.08	9.99 ± 0.11	-0.01
		control	9.74 ± 0.43		10.00 ± 0.18	
41.25 – 42.0	4	AGN	9.43 ± 0.64	− 0.55	9.94 ± 0.64	-0.14
		control	9.98 ± 0.15		10.08 ± 0.03	

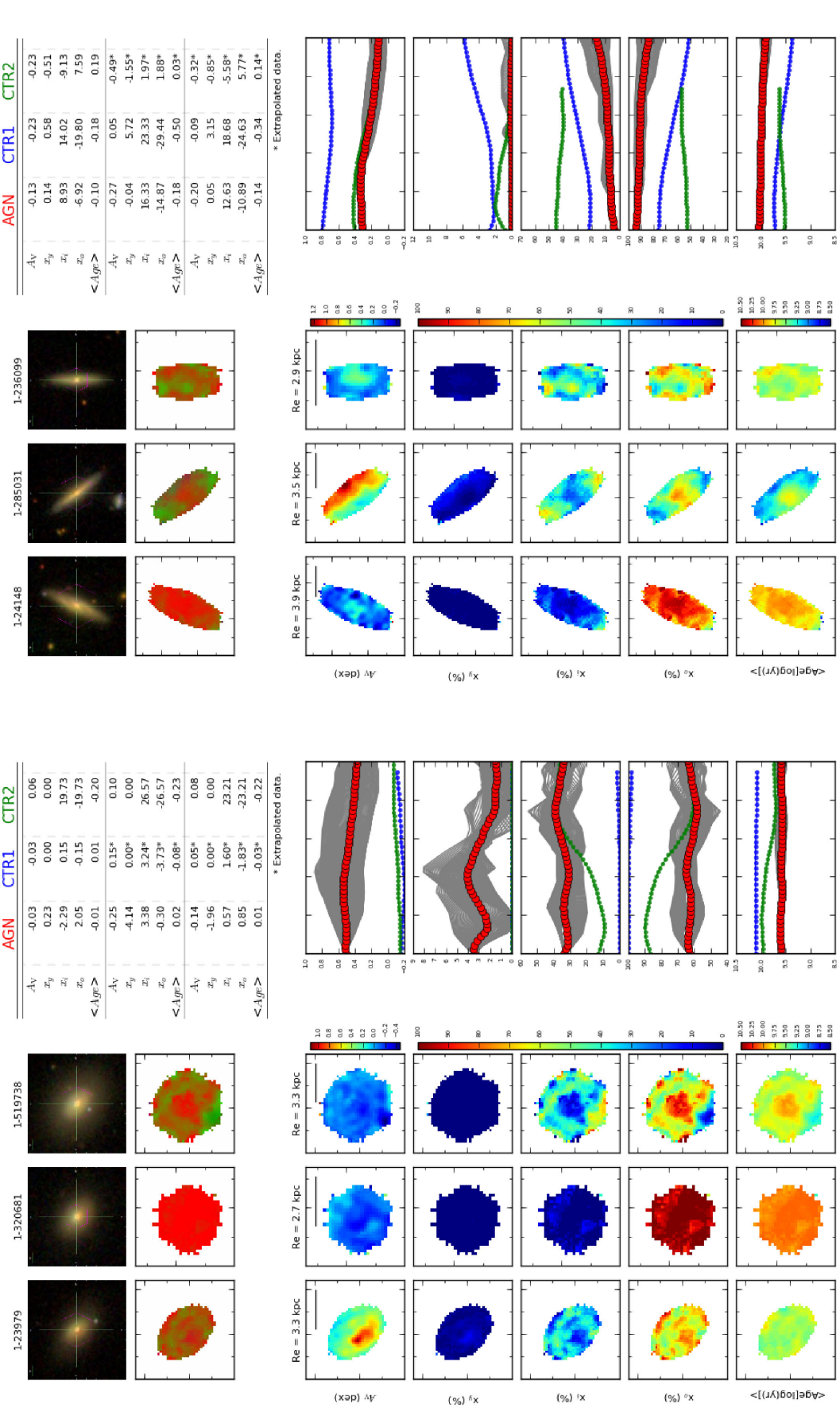

Figure 11. Comparison between the spatially resolved stellar population of an AGN (first column) and its two control galaxies (second and third columns). Top left-hand panel: two rows of panels, SDSS image of the galaxies (top) and RGB maps (bottom) showing the relative percent contribution of the young (<40 Myr, blue), intermediate age (50Myr–2 Gyr, green) and old (> 2 Gyr, red) stellar population. Top right-hand panel: table summarizing the average gradient values for the different properties calculated at three effective radius ranges (0.0–0.5, 0.5–1.0 and 0.0–1.0R_e) using the mean profiles shown. Bottom panel: five rows of panels, from the top to bottom: visual extinction A_V, percent contribution of the young (x_y), intermediate age (x_i) and old (x_o), and average age (<*Age*>). Fourth column: mean profiles of the properties shown in the left figures, as a function of effective radius. Active galaxy in red, control galaxies in blue and green. Grey lines show the profiles of the active galaxy for each sector of 35° (see further explanations in the text). For display purposes, we used tick marks separated by 5 arcsec. The solid horizontal line in the A_V maps represent 5 kpc.

our synthesis result for the inner pixel was consistent with that obtained from the SDSS-III spectra. We concluded that the results were the same within the uncertainties, as expected.

The resolved synthesis (beyond the inner $\sim$ 1.5 arcsec) will be discussed in Paper II, and preliminary results are shown in Fig. 11 for two sets of AGN and control sample galaxies: the first set corresponds to an early-type host and the second to a late-type host. The area covered by the central fibre of the MaNGA array, at the mean distance of these galaxies, is around 1.5 kpc. In these figures, we have further collapsed the ages in three bins: young (x_y, $t < 10$ Myr), intermediate age (x_i, 51 Myr $\leq t \leq$ 2 Gyr) and old (x_o, $t > 2$ Gyr). In the case of the early-type galaxy, it can be seen that the AGN host has (1) a stronger reddening over the whole galaxy than the two control galaxies, suggesting the presence of more gas in the AGN host galaxy; (2) a larger contribution of the young component; (3) a larger contribution of the intermediate age component in the inner region and then it becomes similar to that of the second control galaxy (green) outwards; (4) a smaller contribution of the old component everywhere in the galaxy, being approximately the same as that of the second control galaxy in the outer part of the galaxy; and (5) an average age that is smaller than those of the two controls in the inner region and similar to that of the second control in the outer parts of the galaxy.

In the case of the late-type galaxy, the AGN host has (1) a similar reddening to that of the second control galaxy, being smaller than that of the first control galaxy; (2) a lower contribution of the young component than the first control everywhere, a lower contribution than the second control in the inner parts but similar outwards; (3) a smaller contribution of the intermediate-age component to that of the controls everywhere; and (4) a larger contribution of the old component everywhere and a (5) a larger mean age everywhere.

In summary, we have find a difference in the resolved stellar population properties between the AGN and control galaxies for the early-type AGN host and found no difference in the late-type AGN host. We note that the difference between the stellar population of the early-type AGN host and those of the control galaxies is not restricted to the nucleus, but is observed out to about 0.6 effective radii. In Paper II, we will present the results for the whole sample, as well as a statistical analysis to investigate the difference between the AGN and control sample in terms of their resolved stellar population properties.

5 CONCLUSIONS

We have characterized the first 62 AGN host galaxies observed in the MaNGA survey, defining and also characterizing a control sample of 2 galaxies for each AGN, matched according to global properties of the host galaxy such as stellar mass, distance, inclination and galaxy type. We compare the stellar population properties of the two samples within the inner $\sim$ 1.5 arcsec radius around the nucleus (1–3 kpc at their typical distances) using stellar population synthesis of their SDSS-III spectra and the central spectrum of the MaNGA array, which are identical within the uncertainties. This study will be followed by the study of the resolved stellar population (Paper II) and gas properties (Paper III) over the whole region of the galaxy covered by the MaNGA observations.

The main results of this paper are as follows:

(i) The stellar mass, redshift, *r*-band absolute magnitude, concentration and asymmetry distributions of the AGN hosts are well matched by those of the control sample. The galaxy morphologies are similar, with $\approx$65 per cent spiral and $\approx$33 per cent spheroidal galaxies. The luminosity L([O III]), however, is markedly lower ($\sim$1.4 dex) for the control sample galaxies, as expected.

(ii) Only 17 AGNs of our sample have AGN luminosities larger than $L([\mathrm{O\,III}]) \geq 3.8 \times 10^{40}\,\mathrm{erg\,s^{-1}}$ (which we call strong AGN). Of these, three show signs of disturbed morphology, a much higher proportion than among the remaining, weak AGN.

(iii) The stellar population of the 45 weak AGNs ($L([\mathrm{O\,III}]) < 3.8 \times 10^{40}\,\mathrm{erg\,s^{-1}}$) is dominated (down to 60 per cent contribution to the light at 5700 Å) by old stars (with ages $4.0 \leq t \leq 13.1 \times 10^9$ yr) with a smaller contribution (up to 40 per cent) of intermediate age stars ($0.64 \leq t \leq 2.5 \times 10^9$ yr) and almost no contribution of younger stars; similar results are observed for the control sample;

(iv) The strong AGN, on the other hand, show, on average, a larger contribution (of up to $\approx$ 20 per cent) of younger ($\leq 5 \times 10^7$ yr) stars and a decreased contribution of the old stars relative to both the weak AGN and control sample;

(v) A correlation between the stellar population properties and the AGN luminosity, extending also to lower L[O III] values, is found when pairing each AGN with its controls, via differential properties AGN–control, evidencing the importance in a careful selection of a control sample;

(vi) Via this pairing, we find a correlation between the differential contribution (AGN–control) of the stellar population age component x_{yo} (25–48 $\times$ 10^6 yr) and the AGN luminosity L[O III], and an inverse correlation between the differential contribution of the old age component x_o (4–13 $\times$ 10^9 yr) and L[O III];

(vii) The pairing also reveals a trend in the mean differential age (AGN–control) and the AGN luminosity, in the sense that more luminous AGNs are younger than the control sample. There is also a trend for weak AGNs to be older than the control sample, while those with intermediate luminosity show similar ages to those of the control galaxies.

In summary, our results point to a difference between the stellar population of the AGN hosts and control sample that is correlated with the AGN luminosity: The most luminous the AGN, the younger is its stellar population in the inner kiloparsecs. This result supports the evolutionary scenario (Storchi-Bergmann et al. 2001; Davies et al. 2007) in which episodes of nuclear activity are preceded by episodes of star formation in the galaxy as both star formation and the nuclear activity feed on gas accretion towards the central regions of the galaxy.

In forthcoming papers, we will expand the present investigation to include more AGN as they become observed with MaNGA, studying also the spatially resolved properties of the stellar population (Paper II), the gas excitation (Paper III) and kinematics, as well as the environment of our AGN sample as compared with those of the control sample using the spatially resolved spectroscopic data from MaNGA.

ACKNOWLEDGEMENTS

We would like to thank the support of the Instituto Nacional de Ciência e Tecnologia (INCT) e-Universe project (CNPq grant 465376/2014-2). RAR acknowledges support from FAPERGS (project no. 2366-2551/14-0) and CNPq (project no. 470090/2013-8 and 302683/2013-5). RR thanks to FAPERGS (16/2551-0000251-7) and CNPq for financial support.

Funding for the Sloan Digital Sky Survey IV has been provided by the Alfred P. Sloan Foundation and the Participating Institutions. SDSS-IV acknowledges support and resources from the

Center for High-Performance Computing at the University of Utah. The SDSS web site is www.sdss.org. SDSS-IV is managed by the Astrophysical Research Consortium for the Participating Institutions of the SDSS Collaboration including the Brazilian Participation Group, the Carnegie Institution for Science, Carnegie Mellon University, the Chilean Participation Group, Harvard-Smithsonian Center for Astrophysics, Instituto de Astrofísica de Canarias, The Johns Hopkins University, Kavli Institute for the Physics and Mathematics of the Universe (IPMU) / University of Tokyo, Lawrence Berkeley National Laboratory, Leibniz Institut für Astro physik Potsdam (AIP), Max-Planck-Institut für Astrophysik (MPA Garching), Max-Planck-Institut für Extraterrestrische Physik (MPE), Max-Planck-Institut für Astronomie (MPIA Heidelberg), National Astronomical Observatory of China, New Mexico State University, New York University, The Ohio State University, Pennsylvania State University, Shanghai Astronomical Observatory, United Kingdom Participation Group, Universidad Nacional Autónoma de México, University of Arizona, University of Colorado Boulder, University of Portsmouth, University of Utah, University of Washington, University of Wisconsin, Vanderbilt University and Yale University.

REFERENCES

Alam S. et al., 2015, ApJS, 219, 12
Baldwin J. A., Phillips M. M., Terlevich R., 1981, PASP, 93, 5
Balogh M. L., Morris S. L., Yee H. K. C., Carlberg R. G., Ellingson E., 1999, ApJ, 527, 54
Bower R. G., Benson A. J., Malbon R., Helly J. C., Frenk C. S., Baugh C. M., Cole S., Lacey C. G., 2006, MNRAS, 370, 645
Bruzual G., Charlot S., 2003, MNRAS, 344, 1000
Bundy K. et al., 2015, ApJ, 798, 7
Cardelli J. A., Clayton G. C., Mathis J. S., 1989, IAUS, 135, 5
Cardoso L. S. M., Gomes J. M., Papaderos P., 2017, A&A, 604, A99
Cid Fernandes R., Sodré L., Schmitt H. R., Leão J. R. S., 2001, MNRAS, 325, 60
Cid Fernandes R., Gu Q., Melnick J., Terlevich E., Terlevich R., Kunth D., Rodrigues Lacerda R., Joguet B., 2004, MNRAS, 355, 273
Cid Fernandes R., Mateus A., Sodré L., Stasińska G., Gomes J. M., 2005, MNRAS, 358, 363
Cid Fernandes R., Stasińska G., Schlickmann M. S., Mateus A., Vale Asari N., Schoenell W., Sodré L., 2010, MNRAS, 403, 103
Cid Fernandes R. J. Terlevich R., 1995, MNRAS, 272, 423
Conroy C., Gunn J. E., White M., 2009, ApJ, 699, 486
Dametto N. Z., Riffel R., Pastoriza M. G., Rodríguez-Ardila A., Hernandez-Jimenez J. A., Carvalho E. A., 2014, MNRAS, 443, 1754
Davies R., Müller Sánchez F., Genzel R., Tacconi L. J., Hicks E. K. S., Friedrich S., Sternberg A., 2007, ApJ, 671, 1388
Di Matteo T., Springel V., Hernquist L., 2005, Nature, 433, 604
Diamond-Stanic A. M., Rieke G. H., 2012, ApJ, 746, 168
Drory N. et al., 2015, AJ, 149, 77
Dubois Y., Gavazzi R., Peirani S., Silk J., 2013, MNRAS, 433, 3297
Eisenstein D. J. et al., 2011, AJ, 142, 72
Esquej P. et al., 2014, ApJ, 780, 86
Fabian A., 2012, ARA&A, 50, 455
Ferrarese L., Ford H. C., 2005, Space Sci. Rev., 116, 523
Ferrarese L., Merrit D., 2000, ApJ, 547, 140
Fukugita M., Ichikawa T., Gunn J. E., Doi M., Shimasaku K., Schneider D. P., 1996, AJ, 111, 1748
Gebhardt K. et al., 2000, ApJ, 539, 13
Gunn J. E. et al., 2006, AJ, 131, 2332
Heckman T. M., González-Delgado R., Leitherer C., Meurer G. R., Krolik J., Wilson A. S., Koratkar A., Kinney A., 1997, ApJ, 482, 114
Hickox R. C., Mullaney J. R., Alexander D. M., Chen C.-T. J., Civano F. M., Goulding A. D., Hainline K. N., 2014, ApJ, 782, 9
Ishibashi W., Fabian A. C., 2014, MNRAS, 441, 1474
Jahnke K., Macciò A. V., 2011, ApJ, 734, 92
Kauffmann G., Heckman T. M., Tremonti C. et al., 2003, MNRAS, 346, 1055
Kewley L. J., Dopita M. A., Sutherland R. S., Heisler C. A., Trevena J., 2001, ApJ, 556, 121
Kormendy J., Ho L. C., 2013, ARA&A, 51, 511
Koski A. T., 1978, ApJ, 223, 56
Law D. R. et al., 2015, AJ, 150, 19
Law D. R. et al., 2016, AJ, 152, 83
Lintott C. et al., 2011, MNRAS, 410, 166
Mazzalay X., Rodríguez-Ardila A., Komossa S., 2010, MNRAS, 405, 1315
Menanteau F., Ford H. C., Motta V., Benítez N., Martel A. R., Blakeslee J. P., Infante L., 2005, AJ, 131, 208
Müller-Sánchez F., Prieto M. A., Hicks E. K. S., Vives-Arias H., Davies R. I., Malkan M., Tacconi L. J., Genzel R., 2011, ApJ, 739, 69
Nemmen R., Bower R., Babul A., Storchi-Bergmann T., 2007, MNRAS, 377, 1652
Norman C., Scoville N., 1988, ApJ, 332, 124
Peng C. Y., 2007, ApJ, 671, 1098
Perry J. J., Dyson J. E., 1985, MNRAS, 213, 665
Pontzen A., Tremmel M., Roth N., Peiris H. V., Saintonge A., Volonteri M., Quinn T., Governato F., 2017, MNRAS, 465, 547
Riffel R., Pastoriza M. G., Rodríguez-Ardila A., Bonatto C., 2009, MNRAS, 400, 273
Rodríguez-Ardila A., Prieto M. A., Portilla J. G., Tejeiro J. M., 2011, ApJ, 743, 100
Smee S. A. et al., 2013, AJ, 126, 32
Somerville R. S., Hopkins P. F., Cox T. J., Robertson B. E., Hernquist L., 2008, MNRAS, 391, 481
Springel V., Di Matteo T., Hernquist L., 2005, ApJ, 620, 79
Storchi-Bergmann T., Raimann D., Bica E. L. D., Fraquelli H. A., 2000, ApJ, 544, 747
Storchi-Bergmann T., González Delgado R. M., Schmitt H. R., Cid Fernandes R., Heckman T., 2001, ApJ, 559, 147
Terlevich R., Melnick J., 1985, MNRAS, 213, 841
Terrazas B. A., Bell E. F., Henriques B. M. B., White S. D. M., Cattaneo A., Woo J., 2016, ApJ, 830, L12
Thomas D. et al., 2013, MNRAS, 431, 1383
Wild V., Heckman T., Charlot S., 2010, MNRAS, 405, 933
Worthey G., 1994, ApJS, 95, 107
Xie F., Yuan F., Ho L. C., 2017, ApJ, 844, 42
Yan R. et al., 2016, AJ, 151, 8
York D. G. et al., 2000, AJ, 120, 1579
Zakamska N., Greene J., 2014, MNRAS, 442, 784

SUPPORTING INFORMATION

Supplementary data are available at *MNRAS* online.

appendix.pdf

Please note: Oxford University Press is not responsible for the content or functionality of any supporting materials supplied by the authors. Any queries (other than missing material) should be directed to the corresponding author for the article.

APPENDIX A: DETAILED RESULTS FROM THE STELLAR POPULATION SYNTHESIS

Table A1. Synthesis results for AGN in MaNGA MPL5. (1) galaxy identification in the MaNGA survey; (2) flux contribution of the FC; (3)–(8): percentual of the flux corresponding to each of the six age bins defined in Section 3.1; (9)–(14): mass contribution of the same age bins; (15) visual extinction in magnitudes; (16)–(17): light and mass weighted mean stellar age; (18)–(19): light and mass weighted mean stellar metallicity; and (20): mean relative deviation between the fit and the galaxy spectrum.

mangaID (1)	FC (2)	xyy (3)	xyo (4)	xIy (5)	xII (6)	xIo (7)	xo (8)	myy (9)	myo (10)	mIy (11)	mII (12)	mIo (13)	mo (14)	A_V (15)	$\langle t_L \rangle$ (16)	$\langle t_M \rangle$ (17)	$\langle Z_L \rangle$ (18)	$\langle Z_M \rangle$ (19)	Adev (20)
1-109056	3.38	4.25	0.00	0.00	13.65	0.00	76.37	0.07	0.00	0.00	2.54	0.00	97.39	0.14	9.75	10.07	0.019 57	0.018 64	2.90
1-121532	4.42	4.63	1.96	0.00	17.07	0.00	71.26	0.08	0.06	0.00	2.85	0.00	97.01	0.50	9.70	10.08	0.019 65	0.023 09	5.40
1-135044	7.63	0.00	0.00	0.00	0.00	4.03	85.79	0.00	0.00	0.00	0.00	1.22	98.78	0.14	9.92	10.02	0.017 27	0.018 77	2.58
1-135285	0.04	0.00	0.00	0.00	0.00	0.00	97.15	0.00	0.00	0.00	0.00	0.00	100.00	0.17	10.00	10.07	0.014 75	0.017 61	2.76
1-135641	4.24	2.54	0.00	0.00	9.54	0.00	80.90	0.04	0.00	0.00	1.34	0.00	98.62	0.91	9.88	10.10	0.018 57	0.022 83	2.45
1-137883	0.00	10.51	9.50	0.00	2.28	40.64	34.75	0.16	0.31	0.00	0.62	14.82	84.10	1.58	9.12	9.98	0.014 46	0.027 49	3.28
1-148068	3.61	0.00	0.00	0.00	0.00	13.03	79.76	0.00	0.00	0.00	0.00	3.14	96.86	0.26	9.98	10.08	0.0246	0.024 62	3.86
1-149211	12.13	0.00	0.00	0.00	0.00	49.60	36.05	0.00	0.00	0.00	0.00	27.91	72.09	0.18	9.55	9.83	0.033 61	0.022 62	3.96
1-163831	3.93	1.36	0.00	0.00	0.00	9.75	81.93	0.02	0.00	0.00	0.00	2.32	97.66	0.24	9.90	10.06	0.019 05	0.022 43	3.05
1-166919	4.98	1.72	0.00	0.00	4.70	13.33	72.58	0.03	0.00	0.00	0.83	2.28	96.86	0.23	9.84	10.08	0.019 42	0.019 96	2.39
1-167688	3.56	3.80	1.15	0.00	34.40	25.77	30.48	0.12	0.05	0.00	11.29	10.72	77.83	0.15	9.27	9.87	0.019 05	0.020 04	2.16
1-173958	7.42	16.37	0.85	0.00	19.93	20.47	33.50	0.28	0.02	0.00	6.16	8.44	85.11	0.62	9.05	9.96	0.023 02	0.028 79	3.47
1-198153	0.00	1.69	0.00	0.00	0.00	0.00	96.20	0.02	0.00	0.00	0.00	0.00	99.98	0.41	10.04	10.11	0.014 35	0.016 66	2.63
1-198182	4.95	0.00	0.00	0.00	0.00	0.00	92.01	0.00	0.00	0.00	0.00	0.00	100.00	−0.06	10.11	10.11	0.022 16	0.024 84	1.87
1-201561	4.08	0.00	0.00	0.00	0.00	0.00	91.27	0.00	0.00	0.00	0.00	0.00	100.00	−0.03	10.11	10.11	0.02364	0.02726	3.79
1-209980	17.08	0.00	0.00	0.00	0.00	0.00	81.52	0.00	0.00	0.00	0.00	0.00	100.00	0.03	10.11	10.11	0.016 71	0.018 97	2.00
1-210646	3.37	4.78	0.00	0.00	0.00	18.12	71.64	0.11	0.00	0.00	0.00	7.47	92.42	0.45	9.54	9.92	0.017 84	0.017 77	4.77
1-211311	4.34	0.00	0.00	0.00	0.00	6.11	85.90	0.00	0.00	0.00	0.00	1.67	98.33	−0.02	9.97	10.05	0.0176	0.017 95	2.45
1-217050	1.26	1.12	0.00	0.00	0.00	0.00	94.71	0.01	0.00	0.00	0.00	0.00	99.99	0.00	10.07	10.11	0.020 53	0.0238	1.64
1-22301	7.65	2.15	0.00	0.00	0.00	11.75	74.97	0.02	0.00	0.00	0.00	2.40	97.58	0.18	9.89	10.08	0.018 94	0.0237	2.59
1-229010	2.42	0.00	0.00	0.00	0.00	0.00	93.18	0.00	0.00	0.00	0.00	0.00	100.00	−0.10	10.06	10.09	0.019 87	0.022 36	1.58
1-234618	0.00	3.91	0.00	0.00	2.10	2.29	88.13	0.06	0.00	0.00	0.42	0.61	98.92	0.78	9.78	10.04	0.014 16	0.018 97	5.22
1-23979	1.60	5.66	0.00	0.00	25.10	0.00	65.77	0.10	0.00	0.00	5.11	0.00	94.79	0.54	9.57	10.05	0.025 22	0.021 86	2.63
1-24148	8.51	0.00	0.00	0.00	0.00	5.64	83.67	0.00	0.00	0.00	0.00	1.32	98.68	0.26	10.05	10.10	0.022 32	0.024 33	2.28
1-248389	0.00	3.03	0.00	5.12	11.80	38.14	39.81	0.07	0.00	0.51	2.83	9.95	86.65	0.45	9.41	9.98	0.019 49	0.031 18	1.99
1-248420	9.48	0.00	0.00	0.00	0.00	0.00	87.58	0.00	0.00	0.00	0.00	0.00	100.00	0.18	10.09	10.09	0.014 47	0.015 68	3.07
1-25554	0.00	3.36	0.00	0.00	0.00	34.06	59.68	0.06	0.00	0.00	0.00	9.95	89.99	0.32	9.68	10.03	0.019 57	0.019 02	2.66
1-256446	1.36	0.00	0.00	0.00	0.00	0.00	94.32	0.00	0.00	0.00	0.00	0.00	100.00	−0.04	10.11	10.11	0.017 99	0.019 05	2.96
1-25725	11.87	1.28	0.00	0.00	0.00	0.00	85.18	0.00	0.00	0.00	0.00	0.00	100.00	0.17	10.06	10.11	0.031 77	0.035 29	3.20
1-258599	9.11	13.62	6.83	2.11	14.44	12.09	39.36	0.20	0.22	0.29	5.15	5.75	88.39	0.62	9.01	9.92	0.021 81	0.036 97	3.19
1-258774	1.79	4.81	0.00	0.00	10.70	27.62	51.72	0.04	0.00	0.00	2.43	8.96	88.57	0.41	9.56	10.00	0.027 01	0.0221	2.02
1-259142	3.62	0.00	0.00	0.00	0.00	0.00	92.92	0.00	0.00	0.00	0.00	0.00	100.00	−0.00	10.11	10.11	0.020 69	0.022 18	2.20
1-269632	4.49	18.98	8.39	0.00	37.97	18.93	9.14	0.51	0.50	0.00	24.60	16.72	57.68	0.65	8.61	9.65	0.029 23	0.043 36	3.64
1-277552	0.00	5.96	0.00	0.00	10.34	0.00	79.53	0.10	0.00	0.00	1.55	0.00	98.35	0.64	9.71	10.04	0.018 71	0.0161	4.72
1-279073	5.45	0.00	0.00	0.00	0.00	0.00	90.99	0.00	0.00	0.00	0.00	0.00	100.00	−0.13	10.11	10.11	0.026 47	0.029 96	2.19
1-279147	5.08	5.23	0.00	0.00	18.03	37.63	31.30	0.09	0.00	0.00	6.78	20.13	73.00	0.56	9.25	9.81	0.030 86	0.0274	2.75
1-279666	0.00	3.12	0.00	0.00	7.44	36.36	49.72	0.07	0.00	0.00	1.90	11.48	86.55	0.26	9.54	9.93	0.019 97	0.023 75	2.44
1-279676	0.00	1.99	0.00	0.00	7.49	19.39	69.58	0.03	0.00	0.00	1.48	5.64	92.84	0.32	9.75	10.04	0.024 02	0.018 53	3.36
1-321739	0.00	2.74	2.19	0.00	15.14	9.42	68.96	0.03	0.05	0.00	2.80	2.45	94.67	1.08	9.69	10.06	0.020 29	0.022 71	2.96
1-338922	0.00	14.28	0.00	0.00	0.00	32.92	51.74	0.16	0.00	0.00	0.00	17.42	82.41	0.48	9.33	9.92	0.018 28	0.025 73	6.43
1-339094	7.03	0.00	0.00	0.00	7.66	23.20	59.24	0.00	0.00	0.00	1.90	8.37	89.73	0.29	9.72	9.98	0.024 92	0.019 55	1.86
1-339163	5.93	0.00	0.00	0.00	0.00	0.00	92.23	0.00	0.00	0.00	0.00	0.00	100.00	0.00	10.08	10.10	0.016 74	0.020 13	1.94
1-351790	5.46	2.08	2.60	0.00	43.77	30.59	13.55	0.10	0.16	0.00	22.41	22.30	55.03	0.41	9.16	9.68	0.022 16	0.020 57	2.20
1-37036	0.00	1.59	0.00	0.00	0.00	2.20	93.97	0.02	0.00	0.00	0.00	0.27	99.71	0.22	10.03	10.11	0.018 86	0.022 78	2.11
1-373161	4.82	0.00	0.00	0.00	0.00	0.00	91.52	0.00	0.00	0.00	0.00	0.00	100.00	0.16	10.11	10.11	0.021 99	0.023 94	2.64
1-44303	11.93	1.62	0.00	0.00	4.50	12.94	68.16	0.03	0.00	0.00	1.04	7.58	91.34	0.35	9.82	10.02	0.019 84	0.0175	3.13
1-44379	12.87	0.00	0.00	0.00	0.92	5.16	78.93	0.00	0.00	0.00	0.18	0.87	98.95	0.17	10.04	10.10	0.0124	0.014 33	2.08
1-460812	1.82	1.94	0.00	0.00	0.00	3.39	89.71	0.02	0.00	0.00	0.00	0.78	99.20	0.73	9.92	10.08	0.017 19	0.0231	3.26
1-48116	0.00	6.62	0.00	0.00	17.37	11.44	62.82	0.12	0.00	0.00	3.80	3.19	92.89	0.56	9.54	10.04	0.0195	0.018 76	1.92
1-491229	6.52	0.00	0.00	0.00	0.00	0.00	91.23	0.00	0.00	0.00	0.00	0.00	100.00	0.00	10.11	10.11	0.022 15	0.025 43	2.03
1-519742	2.59	0.00	0.00	0.00	0.00	71.52	23.59	0.00	0.00	0.00	0.00	64.99	35.01	0.26	9.32	9.37	0.033	0.029 45	5.97
1-542318	2.68	0.00	0.00	0.00	0.00	12.83	82.73	0.00	0.00	0.00	0.00	4.09	95.91	0.30	9.99	10.08	0.017 77	0.016 04	4.66
1-558912	11.71	0.00	0.00	0.00	0.00	12.28	72.81	0.00	0.00	0.00	0.00	2.94	97.06	0.03	9.98	10.09	0.027 79	0.026 49	3.45

Table A1. *– continued*

mangaID (1)	FC (2)	xyy (3)	xyo (4)	xIy (5)	xII (6)	xIo (7)	xo (8)	myy (9)	myo (10)	mIy (11)	mII (12)	mIo (13)	mo (14)	A_V (15)	$\langle t_L \rangle$ (16)	$\langle t_M \rangle$ (17)	$\langle Z_L \rangle$ (18)	$\langle Z_M \rangle$ (19)	Adev (20)
1-604761	2.77	0.00	0.00	0.00	0.00	0.00	93.55	0.00	0.00	0.00	0.00	0.00	100.00	0.11	10.11	10.11	0.018 29	0.020 73	2.67
1-72322	16.54	0.00	0.00	0.00	0.00	0.00	80.48	0.00	0.00	0.00	0.00	0.00	100.00	0.19	10.11	10.11	0.028 89	0.030 89	3.34
1-91016	0.00	4.63	0.00	0.00	0.00	56.04	37.49	0.11	0.00	0.00	0.00	29.37	70.52	0.70	9.37	9.75	0.019 53	0.023 14	4.36
1-92866	0.00	1.29	0.00	0.00	0.00	0.00	95.45	0.02	0.00	0.00	0.00	0.00	99.98	0.32	10.02	10.10	0.019 64	0.022 29	2.97
1-94604	9.35	0.00	0.00	0.00	0.00	13.18	74.83	0.00	0.00	0.00	0.00	7.74	92.26	−0.01	9.82	9.97	0.020 21	0.02463	3.16
1-94784	2.90	0.00	0.00	0.00	0.00	36.69	55.88	0.00	0.00	0.00	0.00	12.99	87.01	0.24	9.68	9.95	0.029 94	0.02287	2.13
1-95092	0.00	3.74	0.00	0.00	11.56	0.00	82.36	0.03	0.00	0.00	2.06	0.00	97.91	0.39	9.75	10.06	0.020 84	0.0195	2.03
1-95585	4.16	0.00	0.00	0.00	0.00	0.63	91.02	0.00	0.00	0.00	0.00	0.22	99.78	−0.02	10.11	10.11	0.022 65	0.02563	3.11
1-96075	2.81	6.57	0.00	0.00	0.00	16.27	71.05	0.06	0.00	0.00	0.00	5.30	94.63	0.38	9.63	10.01	0.016 34	0.01836	4.50

Table A2. Synthesis results for the control sample. The columns are the same as in Table A1.

mangaID (1)	FC (2)	xyy (3)	xyo (4)	xIy (5)	xII (6)	xIo (7)	xo (8)	myy (9)	myo (10)	mIy (11)	mII (12)	mIo (13)	mo (14)	A_V (15)	$\langle t_L \rangle$ (16)	$\langle t_M \rangle$ (17)	$\langle Z_L \rangle$ (18)	$\langle Z_M \rangle$ (19)	Adev (20)
1-109493	2.97	0.00	0.00	0.00	0.00	0.00	91.99	0.00	0.00	0.00	0.00	0.00	100.00	−0.15	10.11	10.11	0.0219	0.023 06	3.52
1-114306	1.09	8.07	0.00	0.00	7.78	34.00	46.61	0.13	0.00	0.00	2.22	12.92	84.73	0.44	9.39	9.95	0.014 19	0.0174	4.47
1-121717	0.00	4.42	0.00	0.00	4.38	32.26	56.85	0.07	0.00	0.00	0.88	8.77	90.28	0.53	9.63	10.03	0.018 83	0.021 78	3.11
1-134239	0.00	0.00	0.00	0.00	0.00	14.05	82.24	0.00	0.00	0.00	0.00	3.52	96.48	0.11	9.91	10.06	0.022 97	0.021 96	3.03
1-135371	0.00	2.66	0.00	0.00	14.05	0.00	82.30	0.02	0.00	0.00	2.41	0.00	97.57	0.65	9.84	10.09	0.021 58	0.020 76	2.76
1-135372	0.00	0.00	3.19	0.00	0.00	0.00	96.37	0.00	0.05	0.00	0.00	0.00	99.95	0.02	10.03	10.11	0.019 41	0.0215	1.69
1-135502	0.60	0.00	0.00	0.00	0.00	0.00	94.52	0.00	0.00	0.00	0.00	0.00	100.00	0.13	10.03	10.08	0.017 67	0.020 35	2.18
1-135625	12.87	2.50	12.97	0.00	33.15	18.44	17.30	0.10	0.60	0.00	15.10	11.27	72.93	0.35	8.97	9.82	0.030 15	0.038 99	1.75
1-135810	0.00	0.00	0.00	0.00	0.00	41.05	57.21	0.00	0.00	0.00	0.00	16.27	83.73	0.30	9.61	9.89	0.028 52	0.022 37	2.64
1-136125	0.00	0.00	0.00	0.00	0.00	36.16	60.24	0.00	0.00	0.00	0.00	13.23	86.77	0.29	9.66	9.93	0.027 61	0.0219	4.52
1-166691	0.59	1.18	0.00	0.00	0.00	7.98	86.24	0.01	0.00	0.00	0.00	1.53	98.46	−0.14	10.00	10.10	0.022 01	0.025 57	3.00
1-166947	3.68	0.00	0.00	0.00	0.00	0.00	92.37	0.00	0.00	0.00	0.00	0.00	100.00	−0.10	10.11	10.11	0.021 98	0.025 28	3.27
1-167334	0.00	3.03	0.00	0.00	56.89	36.57	1.18	0.11	0.00	0.00	49.04	42.99	7.86	0.55	9.04	9.20	0.036 21	0.034 18	1.65
1-177493	3.34	0.00	0.00	0.00	0.00	19.37	74.21	0.00	0.00	0.00	0.00	5.77	94.23	0.03	9.82	10.02	0.023 38	0.021 86	2.30
1-178838	12.76	0.00	0.00	0.00	3.31	17.56	62.46	0.00	0.00	0.00	0.62	4.47	94.91	−0.12	9.91	10.07	0.022 77	0.024 85	1.94
1-210173	5.84	0.00	0.00	0.00	2.29	31.23	55.48	0.00	0.00	0.00	0.33	10.10	89.57	0.24	9.74	10.00	0.0307	0.024 89	4.72
1-210593	0.00	0.00	0.00	0.00	6.32	0.00	91.27	0.00	0.00	0.00	1.07	0.00	98.93	0.28	9.91	10.05	0.0209	0.025 03	3.43
1-210614	0.00	1.24	0.00	0.00	0.00	0.00	94.97	0.01	0.00	0.00	0.00	0.00	99.98	0.09	10.06	10.11	0.020 04	0.022 73	2.48
1-210700	0.00	0.00	0.00	0.00	0.00	0.00	96.81	0.00	0.00	0.00	0.00	0.00	100.00	0.16	10.09	10.11	0.023 69	0.02721	5.73
1-210784	0.00	2.87	0.00	0.00	1.19	4.69	88.16	0.03	0.00	0.00	0.11	0.56	99.29	0.11	9.93	10.11	0.023 79	0.028 71	2.34
1-210962	0.00	1.41	0.00	0.00	5.66	8.40	81.53	0.02	0.00	0.00	0.89	1.76	97.33	0.15	9.92	10.09	0.020 33	0.021 74	1.64
1-211063	0.00	1.39	0.00	0.00	0.00	18.78	75.78	0.02	0.00	0.00	0.00	4.88	95.10	0.28	9.87	10.07	0.022 86	0.0192	2.32
1-211074	0.00	1.86	0.00	0.00	0.00	0.00	94.99	0.02	0.00	0.00	0.00	0.00	99.97	0.13	10.03	10.11	0.016 27	0.019 25	2.31
1-211079	0.00	0.00	0.00	0.00	5.97	0.00	92.39	0.00	0.00	0.00	0.59	0.00	99.41	0.03	10.03	10.10	0.020 51	0.025 51	1.93
1-211082	0.00	2.26	0.00	0.00	7.17	0.00	88.14	0.02	0.00	0.00	0.99	0.00	98.98	0.23	9.93	10.10	0.025 93	0.026 56	2.23
1-211100	0.00	1.46	0.00	0.00	0.00	0.00	95.79	0.02	0.00	0.00	0.00	0.00	99.98	0.04	10.05	10.11	0.01701	0.020 87	1.85
12-129446	1.31	4.33	0.00	0.00	0.01	40.22	51.60	0.08	0.00	0.00	0.00	12.01	87.91	0.33	9.59	10.01	0.020 53	0.022 09	2.84
1-216958	15.73	0.00	0.00	0.00	13.14	11.64	56.77	0.00	0.00	0.00	2.41	2.68	94.91	−0.08	9.77	10.05	0.026 46	0.027 07	1.60
1-218280	2.44	0.00	0.00	0.00	0.00	0.00	94.10	0.00	0.00	0.00	0.00	0.00	100.00	−0.14	10.11	10.11	0.0209	0.022 64	3.90
1-218427	2.55	0.00	0.00	0.00	0.00	0.00	94.12	0.00	0.00	0.00	0.00	0.00	100.00	−0.11	10.11	10.11	0.021 09	0.022 95	3.88
1-235398	0.00	5.31	0.00	0.00	0.00	17.60	74.64	0.08	0.00	0.00	0.00	5.14	94.78	0.81	9.64	10.01	0.0122	0.017 17	2.83
1-235587	0.00	1.71	0.00	0.00	6.86	0.00	87.88	0.02	0.00	0.00	1.13	0.00	98.85	−0.07	9.92	10.08	0.018 78	0.018 63	2.09
1-236099	3.82	0.00	0.00	0.00	22.14	28.78	42.23	0.00	0.00	0.00	6.66	12.26	81.08	0.23	9.57	9.93	0.027 43	0.019 06	2.65
1-94514	0.00	1.21	0.00	0.00	0.00	13.14	82.88	0.02	0.00	0.00	0.00	3.02	96.96	0.00	9.93	10.08	0.023 84	0.023 02	2.23
1-23731	0.00	1.71	0.00	0.00	0.00	2.08	91.90	0.02	0.00	0.00	0.00	0.45	99.52	0.02	9.93	10.07	0.017 92	0.022 15	2.01
1-24099	0.00	0.91	0.00	0.00	16.33	0.00	80.68	0.01	0.00	0.00	2.69	0.00	97.30	0.02	9.88	10.08	0.0235	0.021 02	1.85
1-24246	6.94	0.00	0.00	0.00	30.11	0.95	58.39	0.00	0.00	0.00	6.37	0.17	93.46	0.18	9.71	10.03	0.0303	0.02221	6.43
1-24416	0.00	1.01	0.00	0.00	0.00	0.00	96.33	0.01	0.00	0.00	0.00	0.00	99.99	0.25	9.97	10.07	0.016 25	0.019 25	1.94
1-245774	0.00	1.23	0.00	0.00	5.15	33.24	57.82	0.02	0.00	0.00	1.06	9.54	89.38	0.07	9.72	10.02	0.021 76	0.020 83	2.58
1-247417	0.00	6.75	0.00	0.00	1.71	53.99	33.94	0.16	0.00	0.00	0.49	21.04	78.30	0.73	9.38	9.94	0.015 49	0.021 87	2.97
1-247456	0.00	5.43	0.00	0.00	9.06	38.44	44.44	0.11	0.00	0.00	2.22	12.55	85.12	0.43	9.49	9.99	0.016 34	0.020 28	3.45

Table A2. *– continued*

mangaID (1)	FC (2)	xyy (3)	xyo (4)	xIy (5)	xII (6)	xIo (7)	xo (8)	myy (9)	myo (10)	mIy (11)	mII (12)	mIo (13)	mo (14)	A_V (15)	$\langle t_L \rangle$ (16)	$\langle t_M \rangle$ (17)	$\langle Z_L \rangle$ (18)	$\langle Z_M \rangle$ (19)	Adev (20)
1-251279	0.00	1.13	0.00	0.00	2.77	11.06	80.72	0.02	0.00	0.00	0.47	2.54	96.97	0.20	9.90	10.07	0.018 19	0.020 16	1.97
1-251871	6.57	0.00	0.00	0.00	0.00	0.00	89.51	0.00	0.00	0.00	0.00	0.00	100.00	0.06	10.11	10.11	0.021 68	0.022 98	5.18
1-256185	2.28	0.00	0.00	0.00	0.00	0.00	93.72	0.00	0.00	0.00	0.00	0.00	100.00	−0.05	10.07	10.10	0.020 02	0.022 11	1.72
1-256465	0.00	0.00	0.00	0.00	0.00	26.71	69.99	0.00	0.00	0.00	0.00	7.31	92.69	−0.10	9.85	10.04	0.026 69	0.022 67	2.58
1-25680	0.00	1.79	0.00	0.00	0.00	0.00	94.25	0.02	0.00	0.00	0.00	0.00	99.98	−0.13	10.01	10.09	0.028 93	0.033 44	2.76
1-25688	0.00	6.03	0.00	0.00	0.00	10.33	80.42	0.08	0.00	0.00	0.00	4.89	95.03	0.33	9.66	10.01	0.017 29	0.018 77	4.50
1-258455	0.00	1.27	0.00	0.00	0.00	0.00	95.81	0.02	0.00	0.00	0.00	0.00	99.98	0.26	9.98	10.08	0.0147	0.018 23	2.76
1-259650	0.00	1.69	0.00	0.00	0.00	0.00	94.87	0.02	0.00	0.00	0.00	0.00	99.98	0.23	10.04	10.11	0.020 89	0.023 88	1.96
1-264513	0.00	9.38	0.00	4.55	15.78	36.93	30.91	0.15	0.00	0.57	5.19	13.71	80.37	0.35	9.15	9.93	0.019 18	0.0212	1.82
1-270160	0.00	1.21	0.00	0.00	0.00	0.00	94.65	0.01	0.00	0.00	0.00	0.00	99.99	0.39	10.06	10.11	0.024 02	0.027 61	3.05
1-274646	0.43	2.52	0.67	0.00	15.02	52.28	25.36	0.04	0.02	0.00	5.27	25.68	68.98	0.41	9.33	9.81	0.034 76	0.027 03	1.93
1-274663	1.97	0.00	0.00	0.00	0.00	0.00	95.14	0.00	0.00	0.00	0.00	0.00	100.00	0.07	10.11	10.11	0.017 07	0.018 98	1.61
1-276679	15.39	4.90	0.00	0.00	22.42	42.50	13.72	0.08	0.00	0.00	14.85	38.57	46.50	0.32	9.14	9.48	0.028 79	0.033 68	5.12
1-282144	13.94	8.05	0.00	0.00	8.22	57.94	10.42	0.36	0.00	0.00	4.98	53.94	40.72	0.69	9.06	9.48	0.01918	0.0306	6.20
1-283246	0.00	0.00	0.00	0.00	0.00	31.06	64.84	0.00	0.00	0.00	0.00	10.34	89.66	−0.01	9.72	9.95	0.0276	0.022 02	2.83
1-285031	0.00	9.10	0.00	0.00	18.70	0.00	72.37	0.12	0.00	0.00	3.13	0.00	96.75	0.88	9.57	10.07	0.013 09	0.013 18	2.50
1-285052	0.00	1.84	0.00	0.00	6.78	0.00	87.30	0.01	0.00	0.00	1.06	0.00	98.92	0.12	9.95	10.10	0.0202	0.019 98	3.31
1-210785	0.00	2.36	0.00	0.00	5.12	7.49	81.03	0.01	0.00	0.00	0.83	1.62	97.54	0.00	9.91	10.09	0.019 56	0.021 66	1.97
1-286804	0.00	0.00	8.24	16.66	24.32	42.92	5.58	0.00	0.79	5.34	20.46	48.78	24.63	0.33	8.95	9.34	0.028 39	0.027 56	3.96
1-289865	2.24	0.00	0.00	0.00	0.00	0.00	94.47	0.00	0.00	0.00	0.00	0.00	100.00	−0.21	10.08	10.10	0.022 69	0.026 28	1.70
1-295095	2.49	0.00	0.00	0.00	0.00	37.87	56.60	0.00	0.00	0.00	0.00	14.38	85.62	0.07	9.69	9.95	0.0273	0.0198	3.53
1-320681	0.00	0.00	0.00	0.00	0.00	10.53	85.98	0.00	0.00	0.00	0.00	1.25	98.75	−0.07	10.01	10.10	0.025 25	0.029 42	1.70
1-338828	0.00	16.73	7.73	0.00	8.65	58.85	7.16	0.43	0.44	0.00	5.37	51.09	42.67	1.00	8.78	9.58	0.024 18	0.037 73	4.30
1-339028	2.72	0.00	0.00	0.00	0.00	0.00	94.05	0.00	0.00	0.00	0.00	0.00	100.00	−0.08	10.11	10.11	0.023 26	0.026 11	2.33
1-339125	0.00	1.99	0.00	0.00	0.00	0.57	94.78	0.01	0.00	0.00	0.00	0.07	99.92	0.41	10.02	10.11	0.017 08	0.020 65	3.18
1-351538	7.68	2.73	0.00	0.00	6.55	26.05	53.68	0.05	0.00	0.00	1.18	7.80	90.97	0.32	9.65	10.03	0.024 09	0.0241	3.94
1-36878	0.00	8.72	0.00	2.05	13.83	45.19	27.80	0.17	0.00	0.26	4.55	19.97	75.05	0.84	9.25	9.90	0.018 82	0.023 83	2.21
1-37062	1.96	5.04	18.39	0.00	32.06	16.55	23.61	0.08	0.70	0.00	12.73	8.76	77.73	0.77	8.88	9.88	0.025 67	0.028 12	2.35
1-37079	15.94	4.62	0.00	0.00	0.00	59.29	17.37	0.13	0.00	0.00	0.00	57.50	42.37	0.06	9.25	9.46	0.024 14	0.029 46	7.75
1-377125	12.64	0.00	0.00	0.00	0.00	31.51	53.78	0.00	0.00	0.00	0.00	10.73	89.27	0.16	9.77	10.01	0.035 76	0.030 91	4.22
1-377321	21.35	27.63	0.00	15.90	0.00	25.58	7.92	1.34	0.00	5.66	0.00	25.86	67.14	0.20	8.28	9.71	0.012 03	0.035 79	2.33
1-378401	0.00	0.00	0.00	1.58	0.00	0.00	95.58	0.00	0.00	0.08	0.00	0.00	99.92	−0.05	10.09	10.11	0.027 69	0.030 87	2.46
1-378795	1.69	0.00	0.00	0.00	0.00	12.23	81.65	0.00	0.00	0.00	0.00	3.13	96.87	0.24	9.93	10.06	0.021 49	0.02	3.81
1-379087	15.45	5.06	3.25	0.00	4.42	21.55	47.54	0.06	0.08	0.00	1.19	7.48	91.19	0.37	9.51	10.02	0.016 31	0.023 29	2.87
1-379660	0.00	1.11	0.00	0.00	36.10	12.52	47.77	0.02	0.00	0.00	9.50	4.45	86.03	0.45	9.50	9.94	0.028 92	0.023 31	1.66
1-386452	0.00	5.48	0.00	2.46	7.83	40.57	41.26	0.11	0.00	0.23	1.97	13.57	84.12	0.30	9.45	9.98	0.0168	0.023 26	1.60
1-386695	19.61	24.78	0.00	9.17	0.00	30.32	15.10	0.78	0.00	2.01	0.00	17.65	79.55	0.14	8.55	9.89	0.015 86	0.033 72	3.29
1-392976	1.90	0.00	0.00	0.00	0.00	8.78	87.13	0.00	0.00	0.00	0.00	2.95	97.05	0.08	9.93	10.04	0.016 36	0.016 99	3.38
1-322671	0.00	0.00	0.00	0.00	0.00	32.03	63.35	0.00	0.00	0.00	0.00	9.53	90.47	0.00	9.76	9.99	0.029 73	0.0227	2.53
1-43009	9.00	0.00	0.00	0.00	0.00	37.60	52.89	0.00	0.00	0.00	0.00	14.31	85.69	0.31	9.68	9.90	0.020 34	0.022 92	4.45
1-43721	4.01	0.00	0.00	0.00	0.00	0.00	94.49	0.00	0.00	0.00	0.00	0.00	100.00	0.14	10.11	10.11	0.026 41	0.030 12	3.26
1-44789	0.00	0.00	0.00	0.00	0.00	0.00	96.11	0.00	0.00	0.00	0.00	0.00	100.00	0.17	10.08	10.10	0.019 43	0.023 04	3.57
1-47499	0.00	1.90	0.00	0.00	11.79	0.00	83.53	0.03	0.00	0.00	2.29	0.00	97.68	0.39	9.78	10.04	0.018 92	0.018 71	2.97
1-48208	0.00	1.62	0.00	0.00	0.00	0.00	94.83	0.02	0.00	0.00	0.00	0.00	99.98	−0.11	10.04	10.11	0.021 53	0.0236	2.06
1-487130	0.00	10.02	0.00	0.00	8.67	51.80	27.75	0.17	0.00	0.00	2.48	25.46	71.89	0.42	9.19	9.86	0.017 24	0.026 32	3.97
1-489649	0.00	0.84	0.00	0.00	0.00	0.00	95.53	0.01	0.00	0.00	0.00	0.00	99.99	0.21	9.99	10.08	0.016 46	0.018 77	2.75
1-491233	0.00	4.43	3.77	3.32	1.99	39.65	43.89	0.07	0.09	0.32	0.51	13.43	85.59	0.60	9.44	9.99	0.014 47	0.021 46	2.67
1-519738	0.00	0.00	0.00	0.00	0.00	15.67	79.93	0.00	0.00	0.00	0.00	3.51	96.49	−0.09	9.97	10.08	0.023 18	0.020 71	1.74
1-52259	3.49	5.53	0.00	0.00	29.55	32.81	26.06	0.17	0.00	0.00	10.76	16.19	72.88	0.43	9.22	9.82	0.028 62	0.030 64	3.23
1-55572	0.00	1.96	0.00	1.96	0.00	0.00	93.04	0.02	0.00	0.10	0.00	0.00	99.88	−0.22	10.00	10.11	0.023 72	0.0266	1.87
1-604048	0.00	2.13	0.00	0.00	18.87	1.09	77.52	0.03	0.00	0.00	3.19	0.30	96.48	0.15	9.78	10.06	0.018 37	0.017 27	1.70
1-613211	0.00	1.37	0.00	0.33	0.00	0.00	94.87	0.01	0.00	0.02	0.00	0.00	99.97	−0.04	10.05	10.11	0.028 66	0.031 07	2.14
1-626830	0.00	1.90	0.00	3.56	26.07	10.95	55.32	0.02	0.00	0.34	6.63	3.71	89.28	0.55	9.51	9.96	0.025 13	0.024 35	2.59
1-322074	0.00	0.00	0.00	0.00	0.00	39.98	56.43	0.00	0.00	0.00	0.00	13.89	86.11	0.08	9.72	9.98	0.028 35	0.019 69	2.49
1-633990	7.36	22.54	0.00	0.00	0.00	37.91	30.08	0.29	0.00	0.00	0.00	17.12	82.58	0.56	9.04	9.98	0.014 28	0.028 67	2.98
1-633994	0.00	1.49	0.00	0.00	10.82	9.43	75.39	0.01	0.00	0.00	2.01	2.57	95.41	1.19	9.80	10.05	0.0248	0.023 87	3.11

Table A2. *– continued*

mangaID (1)	FC (2)	xyy (3)	xyo (4)	xIy (5)	xII (6)	xIo (7)	xo (8)	myy (9)	myo (10)	mIy (11)	mII (12)	mIo (13)	mo (14)	A_V (15)	$\langle t_L \rangle$ (16)	$\langle t_M \rangle$ (17)	$\langle Z_L \rangle$ (18)	$\langle Z_M \rangle$ (19)	Adev (20)
1-48053	0.00	4.42	0.00	0.00	0.00	0.00	92.42	0.03	0.00	0.00	0.00	0.00	99.97	0.00	9.96	10.11	0.026 49	0.029 32	1.76
1-635503	0.00	22.47	10.86	0.00	0.00	35.45	32.37	0.39	0.41	0.00	0.00	19.28	79.93	1.15	8.78	9.89	0.010 45	0.028 39	3.25
1-71481	3.01	0.00	0.00	0.00	0.00	2.51	91.76	0.00	0.00	0.00	0.00	0.28	99.72	−0.07	10.09	10.11	0.0274	0.02989	2.22
1-71525	0.00	2.20	0.00	0.00	0.00	0.00	94.16	0.02	0.00	0.00	0.00	0.00	99.98	0.33	9.87	10.05	0.016 12	0.021 06	2.99
1-72914	5.38	0.00	0.00	0.00	0.00	23.39	68.11	0.00	0.00	0.00	0.00	5.85	94.15	0.19	9.90	10.07	0.021 55	0.022 17	3.35
1-72928	0.00	0.00	0.00	0.00	0.00	0.00	96.34	0.00	0.00	0.00	0.00	0.00	100.00	−0.14	10.06	10.10	0.022 21	0.025 26	2.31
1-73005	0.00	0.00	0.00	0.00	17.26	39.48	41.22	0.00	0.00	0.00	4.85	14.80	80.35	0.32	9.60	9.93	0.017 82	0.018 43	2.85
1-90849	4.99	0.00	0.00	0.00	18.92	1.51	70.51	0.00	0.00	0.00	3.84	0.45	95.70	0.24	9.81	10.05	0.023 69	0.019 37	3.30
1-92626	1.70	0.65	0.00	0.00	0.00	0.00	92.91	0.01	0.00	0.00	0.00	0.00	99.99	0.03	10.04	10.10	0.022 73	0.026 75	2.69
1-93876	4.73	0.00	0.00	0.00	0.00	20.53	71.66	0.00	0.00	0.00	0.00	5.07	94.93	−0.08	9.89	10.05	0.029 99	0.027 18	3.64
1-94422	3.24	0.00	0.00	0.00	0.00	25.12	67.74	0.00	0.00	0.00	0.00	6.84	93.16	0.17	9.83	10.04	0.029 05	0.0258	2.86
1-94554	4.48	0.00	0.00	0.00	0.00	5.49	86.38	0.00	0.00	0.00	0.00	1.08	98.92	0.01	10.07	10.11	0.021 74	0.024 48	2.25

This paper has been typeset from a TEX/LATEX file prepared by the author.